Engineering Applications of Artificial Intelligence 73 (2018) 50–67

Contents lists available at ScienceDirect

Engineering Applications of Artificial Intelligence

journal homepage: www.elsevier.com/locate/engappai

A survey on automated melanoma detection

Erdem Okur [a], Mehmet Turkan [b,*]

[a] Department of Software Engineering, Izmir University of Economics, Izmir, Turkey
[b] Department of Electrical and Electronics Engineering, Izmir University of Economics, Izmir, Turkey

ARTICLE INFO

Keywords:
Melanoma detection
Skin cancer
Automated detection
Dermoscopy
Image processing
Machine learning

ABSTRACT

Skin cancer is defined as the rapid growth of skin cells due to DNA damage that cannot be repaired. *Melanoma* is one of the deadliest types of skin cancer, which originates from melanocytes. While other skin cancer types have limited spreading capabilities, the danger of melanoma comes from its ability to spread (metastasize) rapidly. Fortunately, it can be detected by visual inspection of the skin surface, and it is 100% curable if identified in the early stages. However, detection by "subjective visual inspection" creates an important problem, due to investigators' different levels of experiences and education. Dermoscopy (dermatoscopy) has significantly increased the diagnostic accuracy of melanoma since late 90's. In addition, several systems have been proposed in order to assist investigators or to perform an automatic melanoma detection. This survey focuses on the algorithms for automated melanoma detection in dermoscopic images through an extensive analysis of the stages in methodologies proposed in the literature, and by examining related concepts and describing possible future directions through open problems in this domain of research.

1. Introduction

Skin cancer is the most common type among all cancers (Mayoclinic, 2017a; Cancer.Org, 2017a; Bethesda Cancer, 2017). In Europe, the number of new skin cancer cases was 100,339 in 2012, of which 22,199 resulted in death (IARC, 2017). In the USA, the number of new skin cancer cases is more than the total number of all other (e.g., breast, lung, prostate and colon) cancer incidences in each year, and the number of estimated new cases diagnosed in 2017 is 87,110 (Cancer.Org, 2017b; SkinCancer.Org, 2017). In each year, two to three million new non-melanoma and 132,000 new melanoma type skin cancer cases occur, according to World Health Organization (WHO) (WHO, 2017). As seen, "melanoma" cases are analyzed separately in these statistics. There is an important reason for such segregation; melanoma is the most dangerous form of skin cancer, and it is considered the most deadly. Although statistical studies show that only 2% of all skin cancer cases are melanoma, it accounts for 75% of all skin cancer deaths (Melanoma.Org, 2017). A detailed examination of general case-statistics of different countries in the world shows how devastating melanoma is. In Europe, the death rate due to melanoma was reported as one person per 24 min in 2012. Melanoma is considered as the Australia's national cancer, where, after prostate (for men), breast (for women), and bowel cancer, melanoma is the third most common cancer type (Melanoma.Org, 2017). According to statistics cited by SkinCancer.org that in the USA, one person dies of melanoma every 54 min and nearly 9730 people are expected to die of it in 2017 alone (SkinCancer.Org, 2017).

Melanoma starts in pigment cells (melanocytes). As opposed to other skin cancer types, it can spread out (metastasize) over other tissues very rapidly (Medicine Net, 2017). The cancer may metastasize through tissue, lymph system or blood circulation. It can spread only into nearby areas while spreading through tissue; however, it can spread out over other body tissues once it penetrates the lymph system or blood vessels (PDQ Adult Treatment Editorial Board, 2018a). The tissue that melanoma spreads then becomes a cancerous growth, which is difficult to deal with. Fortunately the malignant growth occurs on the skin surface, making detection through a simple visual inspection and a complete cure highly possible, if identified at an early stage. Unfortunately, the stage of a melanoma can only be determined after a suspected lesion (or mole) is excised or biopsied. To determine the stage, four basic features are considered: the tumor thickness (Breslow scale Marghoob et al., 2000), its ulceration, and its spread to lymph nodes or other parts of the body (PDQ Adult Treatment Editorial Board, 2018a). There are five main stages of melanoma, i.e., Stage 0, I (A/B), II (A/B/C), III and IV, and their definitions are summarized in Table 1.

Staging plays an important role in developing an appropriate treatment and determining the prognosis. Several procedures can be applied

* Corresponding author.
E-mail addresses: Erdem.Okur@ieu.edu.tr (E. Okur), Mehmet.Turkan@ieu.edu.tr (M. Turkan).
URLs: http://people.ieu.edu.tr/en/erdemokur (E. Okur), http://people.ieu.edu.tr/en/mehmetturkan (M. Turkan).

https://doi.org/10.1016/j.engappai.2018.04.028
Received 30 October 2017; Received in revised form 27 March 2018; Accepted 30 April 2018

Table 1
Stages of melanoma given by the PDQ Adult Treatment Editorial Board (PDQ Adult Treatment Editorial Board, 2018b) (last update: Jan. 2018) (PDQ Adult Treatment Editorial Board, 2018a).

Stage	Definition
Stage 0	Abnormal melanocytes can be found in the outer layer of the skin (epidermis). These cells may turn into cancer. This stage is also called as "melanoma in situ".
Stage I	Cancer has formed. Considers the thickness and ulceration. This stage is divided into Stage IA and Stage IB. **Stage IA:** Tumor is not greater than 1 mm thick and has no ulceration. Formation of a break on the skin. **Stage IB:** Either, tumor has ulceration but not greater than 1 mm thick or; its thickness is in between 1 mm and 2 mm but has no ulceration.
Stage II	Considers the thickness and ulceration. This stage is divided into Stage IIA, Stage IIB and Stage IIC. **Stage IIA:** Either, tumor has ulceration and greater than 1 mm thick but not greater than 2 mm thick or; its thickness is in between 2 mm and 4 mm but it has no ulceration. **Stage IIB:** Either, tumor has ulceration and greater than 2 mm thick but not greater than 4 mm thick or; its thickness is more than 4 mm but it has no ulceration. **Stage IIC:** Tumor has more than 4 mm thickness and it has ulceration.
Stage III	Considers metastasis. Tumor can have any thickness with or without ulceration. It may be spread to one or more lymph nodes or cancer cells are at least 2 cm away from the primary tumor and may be in between primary tumor and a nearby lymph node in a lymph vessel or there may be smaller tumors around primary tumor on/under the skin in a 2 cm radius.
Stage IV	Cancer may have spread into other parts of the body; lung, brain, liver etc., which can be far away from the primary tumor.

at "staging" such as, further physical examination; lymph node mapping (i.e., a substance is injected near melanoma that can be tracked through lymph ducts and according to the result, a biopsy or a removal operation for lymph nodes can be done); CT scan; PET scan (i.e., patient is injected a radioactive glucose, and tumor cells consumes more glucose than the normal ones and therefore, they show up brighter in the scan); MRI with gadolinium (i.e., tumor cells shows up brighter with gadolinium in magnetic resonance images); and lastly, blood chemistry tests (i.e., Lactate Dehydrogenase (LDH) levels can be checked in the blood sample, and high levels of LDH may indicate melanoma in the body) (PDQ Adult Treatment Editorial Board, 2018a). All these procedure results are finally combined with the biopsy of the suspected lesion, resulting in the stage information. For a melanoma case in Stage III or Stage IV, the removal of the lesion itself is insufficient for treatment. As mentioned before, it is much harder to deal with it at these stages, and it may require treatments such as chemotherapy (Airley, 2009), radiation therapy (Washington and Leaver, 2016), immunotherapy (Naing and Hajjar, 2017), and targeted therapy (Yan et al., 2011; Siegel et al., 2018). Therefore, it is crucial for a patient to get a suspected lesion or mole evaluated for early stage detection.

The way for early detection of melanoma starts with awareness raising in the community. At the moment, there are various facilities and events that can evaluate skin surface lesions and moles. For instance in Turkey, there are 19 visual inspection clinics for melanoma (EuroMelanoma.Org, 2017). There are also several programs available online for making appointments in different clinics around the world. In addition, information is available from the World Wide Web (Kanser.Gov.Tr, 2017; Kanser Vakfi, 2017; Mayoclinic, 2017b). Furthermore, there is also a widely accepted guideline to increase awareness of lesions and moles, the "ABCD(E)'s of Melanoma" (WebMd, 2017; Bad.Org, 2017). This basic guideline explains the **A**symmetry, the **B**order irregularity, the number of different **C**olors, and the **D**iameter features of a lesion or a mole. The "E" here stands for "**E**volution" referring to signs that if the lesion or the mole is growing rapidly. In current studies, the "E" is not considered in the automatic detection concept for melanoma. A person who suspects a lesion or a mole after utilizing the aforementioned guideline should visit a dermatologist or a specialist physician for visual inspection. Following this, the investigator may give advice if an excision is needed. If it is the case, this is a relatively easy and short operation to remove or to completely cure the suspected lesion or mole.

As stated briefly above, melanoma is a very dangerous form of skin cancer, and it can be identified visually by investigators. There is indeed a strong need for automated detection algorithms because of the concept of the "subjectivity" problem. This problem originates from the different experiences and education levels of visual melanoma investigators. An average successful visual inspection accuracy is around 65% (Lee, 2001). This reported relatively low accuracy rate is mostly due to the lack of experience of visual investigators, but also it is related to the patient, who may be in a regular clinic, where an ordinary registrar evaluates the lesion or the mole, rather than a specialized facility.

Dermoscopy has widely been utilized in order to increase the melanoma inspection accuracy. In 1663, dermoscopy originated with Kolhaus (Katsambas et al., 2015), who investigated small vessels with a microscope. Later in 1878, the immersion oil, which is placed between the lesion (or the mole) and the lens, was introduced to his method in order to be able to see the textures of lesions or moles (Senel, 2011). Then, a light source is included in the system which leads to a specialized microscope for skin surface lesions (or moles) that is called as the *dermascope* (*dermatoscope*). Basically, this is a device consisting of a built-in light source and a lens (magnifying glass) to examine the skin surface at from 60x to 100x magnification levels. Visual investigator places the device on the skin surface, with a special gel in-between the lens and the skin, and takes a clear magnified picture of the lesion or the mole.

In 2001, a company called 3Gen manufactured a polarized version of the dermatoscope: DermLite (2017a), and since then, the usage

of dermoscopy has rapidly increased to detect melanoma. Even with these new technological improvements however, successful melanoma inspection accuracy of a visual investigator is increased by from 5% to 30% (Braun et al., 2005a). This means that an experienced investigator can miss a melanoma case by 5% chance, whereas a poorly-experienced one can miss it by 30%. Evidently, after such an inspection, one may undergo an excision operation for no reason, but more importantly, one may continue living with a melanoma, which can metastasize. As a results, still "subjectivity" plays an important role in commenting on what investigators see in dermoscopic images. Therefore, there is a strong need for automated detection systems or aiding tools, as a result of these worldwide statistics, and the subjectivity problem.

This survey mainly aims at pointing out the great importance of melanoma, and its visual and automatic detection methods in dermoscopic images. The basic objective here is to give readers a broad perspective on this subject by extensively analyzing the stages of methodologies proposed in the literature, and by mentioning related concepts and describing possible future directions through open problems in this domain of research. It is very important to comprehend this paper's contribution to successful automated melanoma detection systems and aiding tools, by taking each provided individual stage as a "template" in the referred study. Note also that most of the referred studies here are focused principally on the novelty of their contributions, hence the details of the algorithms are concentrated on these specific stages of melanoma detection. The rest of this paper is organized as follows. Section 2 first introduces the automated melanoma detection concept and then extensively analyses its main stages. Section 3 later discusses recent studies, mentions related topics, and describes possible future directions. Section 4 finally concludes the paper with a brief conclusion.

2. Automated melanoma detection

Automated melanoma detection is a way to diagnose melanoma cases from a lesion of a patient using a system that takes the lesion image as input, processes it, and outputs a respective percentage or direct classification result that indicates the lesion is melanoma or not. Automated detection of melanoma dates back to 1988, and since then different methods have been developed (Day and Barbour, 2000). Some examples of mostly known ones include artificial neural networks (Marin et al., 2015; Ercal et al., 1994), decision trees (Zhou and Song, 2013, 2014), and simple thresholding methods for segmentation (Santy and Joseph, 2015). However, at this time little data was available. The limited number of images that can be reached were either captured by regular cameras, or in the form of digitized slides. This was a problem for two reasons. Firstly, there was insufficient data to train a system to detect a disease with many variations. Secondly, with the data at hand, most of the features on a lesion (textures, borders, etc.) could not be recognized or detected due to the limited technology. The latter especially was a serious matter, even if the developed method did not need a training stage.

The invention of dermascope was a turning point. With dermoscopy, as mentioned in Section 1, dermatologists or visual investigators are be able to capture and collect clearly illuminated and greatly magnified images of a lesion. This progress greatly improved the visual quality of the collected data, and thus solved the second problem mentioned above, by providing more details and significant features in the captured images. After the proliferation of dermascope, publicly available datasets for melanoma emerged in 2000's. Still however, there are only a few publicly available datasets, namely, PH2 (Mendonca et al., 2015), EDRA (Argenziano et al., 2000), and the most recent, International Skin Imaging Collaboration (ISIC) Archive (ISIC, 2017b). With the help of these datasets, studies on automated melanoma detection have recently been accelerated.

There are three major stages to automatically detect a melanoma case from a dermoscopic image. These stages are highly aligned with the clinical observations and features of a lesion that is evaluated by a well-experienced dermatologist during visual inspection. A general overview

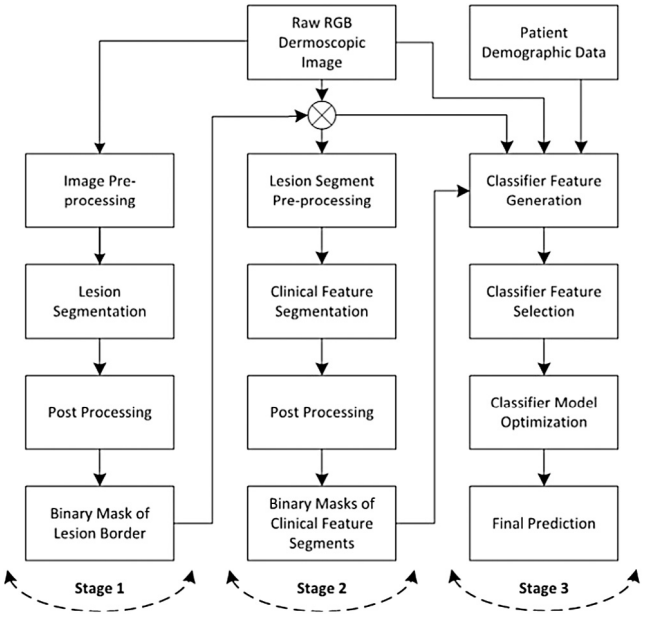

Fig. 1. A block diagram that illustrates three main stages of automated melanoma detection in dermoscopic images (Mishra and Celebi, 2016).

block diagram to the problem is illustrated in Fig. 1 with main stages as (*i*) *lesion segmentation*, (*ii*) *clinical feature segmentation*, and (*iii*) *feature generation, selection, and classification* (Mishra and Celebi, 2016). Please note that trend is rapidly changing and it is indeed evolving over time, hence state-of-the-art methods may not rigidly follow or apply these stages, e.g., some stages might be bypassed or merged. However, it is important to start with a general overview in order to keep this survey coherent, and more importantly, to understand the development of the proposed solutions to the problem of automatic melanoma detection. In the following, each stage as mentioned above will extensively be described more in detail with referrals to the most relevant studies in the literature. Although the main focus will be on the three main stages in Fig. 1, supporting blocks such as "Image Pre-processing" or "Post Processing" will also be mentioned briefly for the respective method used in the relative study.

2.1. *Stage 1 — Lesion segmentation*

Automated melanoma detection starts with lesion segmentation. It is the easiest stage to understand, but also the most important. The success of following stages such that clinical feature segmentation and feature generation for classification is highly dependent on the success of lesion segmentation. In this stage, the lesion is separated from its background (i.e., skin) and other artifacts. One usually ends up with a binary image (or binary mask) that labels the background skin region to be discarded and the lesion region to be further analyzed. Later, clinical features are segmented only on the separated lesion region, from which reveals most of the global features such as (a)symmetry and border (ir)regularity information. A successful example of lesion segmentation is depicted in Fig. 2. On the other hand, a relatively weak segmentation method will probably include background pixels in the lesion segmented region, especially in the close neighborhood of borders. This might lead to erroneous global and local border features, and also to unnecessary color features extracted in the upcoming feature segmentation stage. Various methods have been proposed for lesion segmentation, which is principally an *image segmentation* task. Typical examples are based on thresholding (Garnavi et al., 2011; Celebi et al., 2013), clustering (Schmid, 1999; Mete et al., 2011; Melli et al., 2006), fuzzy logic (Baral et al., 2014), supervised learning (Wu et al., 2013),

Fig. 2. A successful lesion segmentation example: (a) original dermoscopic image, (b) lesion segmented image as a binary mask, and (c) final mask after post-processing (removal of dermascope frame artifacts) (Ogorzalek et al., 2011).

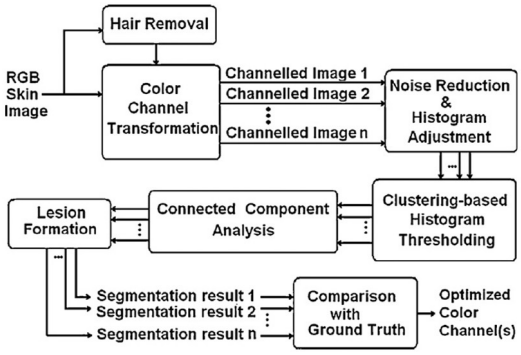

Color channels used in color space transformation.

	Color channel(s)	Color space
1–12	R, G, B, RGB, RoB, GoB, RoG, RoGoB, RGBoR, RGBoG, RGBoB, RGBoRoGoB	RGB
13	I	HSI
14	V	HSV
15	L	LAB
16	Y	YCbCr
17–23	X, Y, Z, XoY, XoZ, YoZ, XoYoZ	XYZ
24–25	XoYoR, XoYoZoR	XYZ and RGB

Fig. 3. The color space optimization system with clustering-based histogram thresholding for lesion segmentation: (left) the block diagram of the optimization procedure, and (right) color channels used in color space transform (Garnavi et al., 2011).

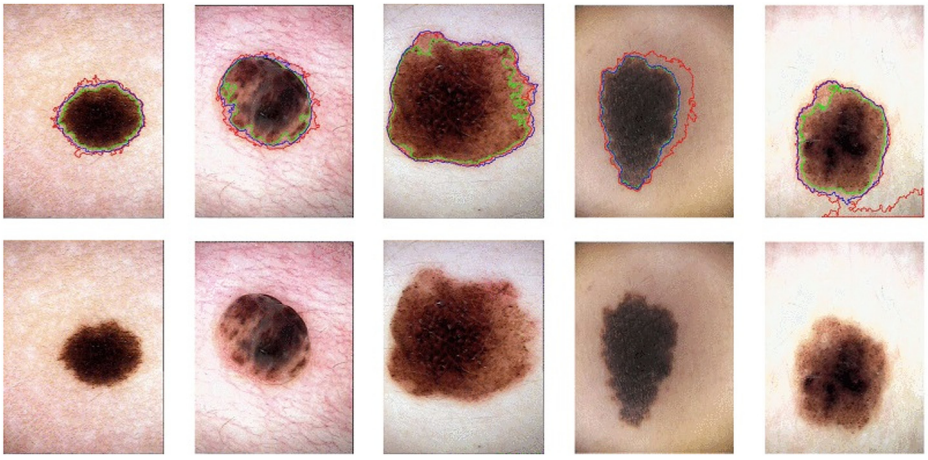

Fig. 4. (Bottom) Original images, and (top) lesion segmentation results: (red borders) adaptive thresholding, (green borders) Otsu's, and (blue borders) results of Yuksel and Borlu (2009). (For interpretation of the references to colour in this figure legend, the reader is referred to the web version of this article.)

and graph theory (Yuan et al., 2009). In addition, some of these methods can be combined to achieve higher segmentation accuracy (Celebi et al., 2009a).

Thresholding (Nobuyuki, 1979; Sezgin and Sankur, 2004) is a very simple and popular method for image segmentation, hence is widely used for lesion segmentation. It basically produces binary images from gray-scale or color images (Shapiro and Stockman, 2002). There are different studies utilizing thresholding, either by combining with different ideas, or by modifying it for lesion segmentation. Garnavi et al. (2011) propose a system to detect lesion borders in which a hybrid method is built with color optimization and clustering-based histogram thresholding. They investigate different color channels in various color spaces in order to obtain the most obvious discrimination between lesion pixels and background skin pixels. In order to do so, 30 dermoscopic color images of lesions are evaluated by 2 dermatologists and 2 dermatology registrars, who manually drew borders around the lesions. After that, 25 color channels from 6 different color spaces (Tkalcic and Tasic, 2003), namely RGB, HSI, HSV, LAB, YCbCr, XYZ (together with a combination of XYZ and RGB), are extracted, and each is processed, as depicted in Fig. 3. Later, results of lesion segmentation are compared with the ground-truth borders drawn by dermatologists and registrars. At the end of this step, the best performing four color channels X, XoYoR, XoYoZoR ("o" stands for logical OR) and R are retained, and the same procedure is repeated with respect to a new reference border that is produced by combining those four manually drawn borders. As a result, the best performing color channels are determined as X and XoYoR, and utilized in a two-step hybrid thresholding method. The overall algorithm is then tested on 85 dermoscopic images, with the result that, in some cases, the proposed scheme has a better mean accuracy than a registrar's border marking by 5.3%, while accepting those of well-experienced dermatologists' as ground-truth. This specific study actually shows the effect of experience that the visual investigator has on the subject. Yuksel and Borlu (2009) propose to use a thresholding method in combination with a type-2 fuzzy logic. After converting the input dermoscopic image into gray-scale, they compute its histogram, from which an optimal threshold value is calculated. This aim is

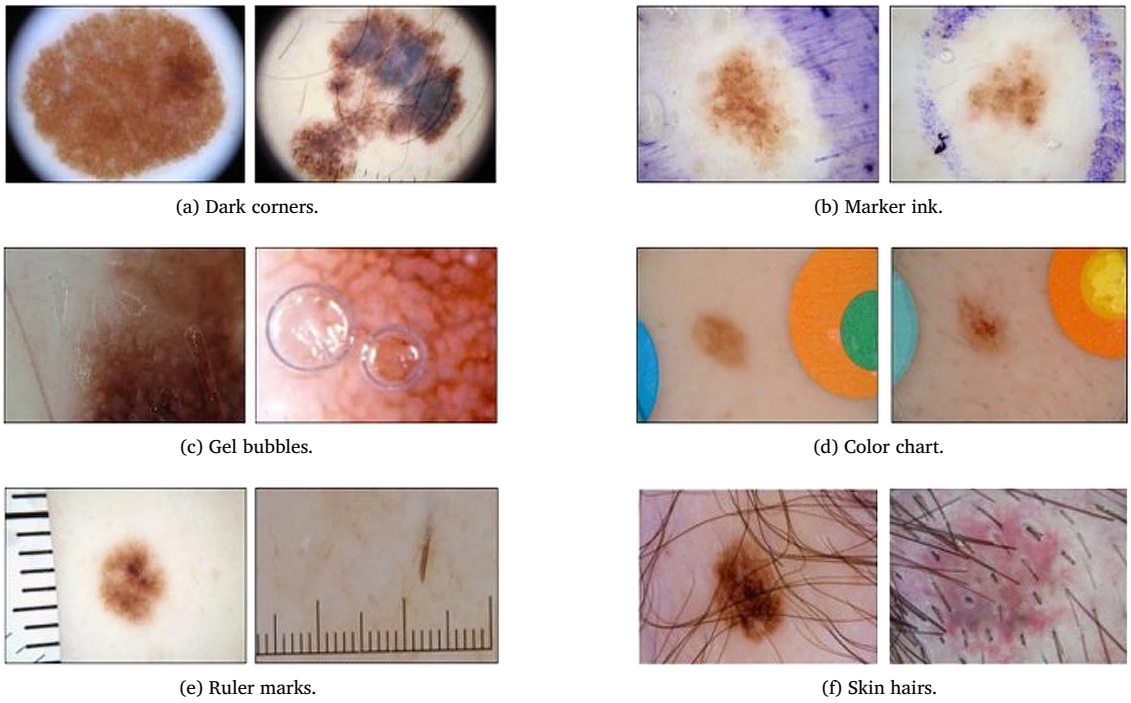

(a) Dark corners. (b) Marker ink.

(c) Gel bubbles. (d) Color chart.

(e) Ruler marks. (f) Skin hairs.

Fig. 5. Typical artifacts contained in dermoscopic images: (a) dark corners, (b) marker ink, (c) gel bubbles, (d) color chart, (e) ruler marks, and (f) skin hairs (Mishra and Celebi, 2016).

accomplished first by deciding a membership function and then by setting its center to the minimum gray-level value. The membership function is later slid across the histogram. The point where the maximum ultrafuzziness (Castillo and Melin, 2008) occurs is finally considered to be the optimal threshold value, and a binary mask is obtained by thresholding the gray-scale image with this value. This method is compared with adaptive thresholding and the most widely used Otsu's method (Nobuyuki, 1979). The authors argue that the Otsu's method creates smaller borders, and the adaptive thresholding method generates larger borders than the actual border size, and furthermore, both Otsu's and adaptive thresholding create artificially more irregular borders than the actual border (ir)regularity. This problem has a critical importance due to the fact that border irregularity is a sign of melanoma. Some example results are given in Fig. 4. In another study, Celebi et al. (2013) define the "Threshold Fusion" as a new method in which ensembles of thresholding techniques are to be used for lesion border detection. While the fusion is mathematically formulated as an energy minimization task, they create an ensemble from four known thresholding methods: Huang and Wang's fuzzy similarity method (Huang and Wang, 1995), Kapur et al.'s maximum entropy method (Kapur et al., 1985), Kittler and Illingworth's minimum error thresholding method (Kittler and Illingworth, 1986), and the Otsu's method (Nobuyuki, 1979). The aim is to obtain comparable results to the best thresholding methods independent from image characteristics. To do so, each of these thresholding algorithms is analyzed in terms of border detection success, based on the main characteristics of the applied image. While noting that Otsu's method gives the least accurate results in some cases, the authors aim to fuse the best performing thresholding methods by adopting the threshold fusion method from Melgani (2006). Their method shows promising thresholding results on 90 dermoscopic test images. It is also fast and easy to implement, and suitable for images that have vessels, skin lines, or tiny hairs, which are regarded as artifacts.

There are various types of artifacts encountered in dermoscopic images. The most problematic matter can be thought of as the physical limitations of the dermoscopic imaging technique. Typical examples include dark corners, marker ink, gel bubbles, color chart, ruler marks, and skin hairs (see Fig. 5). Except skin hairs, artifacts mainly originate from the dermoscopic imaging technique itself. Furthermore, different illumination (lighting), noise, and contrast levels may cloak some very important features in the captured image. Before or after segmenting the lesion region, these artifacts should be dealt with carefully, and eliminated as far as possible. To do so, an image pre-processing on the original image or a post-processing on the segmented lesion, or both, can be applied. A good example of pre-processing for removing skin hairs is DullRazor (Lee et al., 1997). Median filtering is a method of noise reduction and smoothing while removing the skin hair artifacts with pre- or post-processing methods (Mendonca et al., 2015; Lee et al., 1997). In addition, noise reduction (filtering), histogram adjustment, color correction, and contrast enhancement methods can be associated with these supporting blocks, e.g., (Quintana et al., 2009; Wight et al., 2011; Abbas et al., 2013). Region merging (Wong, 2011), border expansion (Iyatomi et al., 2006), and smoothing are examples of frequently utilized techniques in the post-processing side.

Finally, one problem encountered at the lesion segmentation stage that needs a footnote is: *How to evaluate the results of an automated segmentation?* Since it is subjective and highly dependent on the experience of the visual investigator, manual lesion segmentation is problematic by nature. The best approach seems to be the comparison of manual segmentation with the results of the automated ones. Of course, manual segmentation needs to be evaluated on multiple lesions by different experts to get an average perspective. For more details, an exemplary objective evaluation measure study can be found in Celebi et al. (2009b).

2.2. Stage 2 — Clinical feature segmentation

After getting the lesion segmented, a typical melanoma case can be detected by searching for various clinical features which may exist in the segmented region. These features may be global or local. While global features spread over the lesion, local features generally appear on a spot or a group of spots on the lesion. One may group these clinical features into three main categories as *Texture*, *Shape*, and *Color*. In order

to be able to understand these features automatically, different feature extraction techniques can be applied. For example, texture features may be detected with the help of the statistics of the gray-scale version of the input dermoscopic image. A pixel-intensity histogram can be computed, from which the probability distribution of different pixel intensities can be calculated (Hayashi et al., 2005). Other statistical approaches may include not only the pixel intensity values, but also the local pixel-neighboring information (Akram et al., 2015). In addition, some model based methods or spatial domain filtering can also be utilized for texture features (Jamil et al., 2016). For shape features, the most commonly used technique is to check the (a)symmetry feature of the lesion. The (a)symmetric property can easily be detected when the lesion is divided over its principal axes and the two halves do (or, not) match, e.g., (Ng et al., 2005). Finally, color features can be extracted using clustering methods. The basic idea is to cluster and segment color classes defined by dermatologists, e.g., (Schmid, 1999). As an indicator, the number of different colors exist on a lesion can be counted and a threshold can be established for the number of colors for melanoma detection. To sum up here, the main aim of the clinical feature segmentation stage is to detect above named features accurately as possible. Thus, this stage is very similar to lesion segmentation in terms of applicable algorithms and image segmentation methods. The difference is only on the output, since this stage tries to segment the lesion region into several new partitions where specific clinical features are located. The output of the clinical feature segmentation stage can be a (binary) mask that generates a feature when applied on a lesion region. This mask may later be used to generate features to be used with the ultimate classification stage. Alternatively, the output can only be a pixel value of the corresponding feature, or just a binary value representing whether or not the corresponding feature exists. It is worth mentioning here that artifacts on dermoscopic images may naturally still exist at this stage if not completely eliminated in the lesion segmentation stage. Therefore, one may apply the same pre- or post-processing steps for feature segmentation, if needed.

As stated earlier, since this stage is a basic image segmentation problem, the rest of this subsection is devoted to describing the types of clinical features to search for in a lesion region, and to explaining the methods applied in visual inspections by dermatologists. In other words, clinical features located in a lesion can vary, and can have different patterns, and the methods applied by dermatologists at the time of a visual inspection will create a basis for these features (Malvehy et al., 2007; Argenziano et al., 2003; Braun et al., 2005b). Some common examples of features that can indicate melanoma include pigment networks, dots and globules, atypical and typical networks, star-burst pattern, and vascular structures. In addition, a standardization proposal reported in Malvehy et al. (2007) indicates two main steps for clinical feature detection. The first step consists in a general inspection of the lesion, there are visual checks of the features, as detailed in Table 2. If there is at least one melanoma indicating feature detected as "melanocytic lesion", the lesion is then subjected to a second step by the visual investigator. The second step contains four applicable guidelines which will be described and then compared in detail in the remaining part of this subsection.

In Table 2, "melanocytic lesion" refers to the inspected lesion occurred due to proliferation of melanocytes and may be suspected to become melanoma. "Saborrheic keratosis" are harmless wart-like lesions that can look like pre-cancerous growth but in fact are normal. "Basal cell carcinoma" is a type of a skin cancer which metastasizes only in very rare cases, with lesions that look like red patches, open sores or pink growths. "Vascular lesion" is another class of lesions, usually benign, but can sometimes be visually challenging, depending on its type.

2.2.1. Pattern analysis criteria

Pattern Analysis Criteria is a guideline in which enables searches of global and local features on the suspected lesion. As a second step here, the features searched are basically detailed sub-classes of the features detected in the first step. Depending on the feature and its pattern, or the combinations of different types of the same feature, the diagnostic may indicate melanoma. Global and local features and their indications are detailed in Table 3.

In Table 3, "melanocytic nevus" refers to benign lesions which include melanocytes. "Dermal nevus" are melanocytic lesions, which are mostly benign, and they rest on the dermis. "Spitz/Reed nevus" are melanocytic lesions which closely resemble melanoma, and some may metastasize. "Acral nevus" are harmless lesions located on palms or soles, and are generally smaller.

2.2.2. ABCD rule

As a guideline for the community, the famous ABCD Rule depends on four characteristics of a lesion, namely A, B, C, D, as described in Section 1. There is a variant for visual investigators; however, it is slightly different. The first difference is the definition of "D". "D" stands for diameter (dimension) in the community guideline, whereas investigator-version defines it as "dermoscopic structures". These structures can be the presence of different networks, structureless areas, globules, streaks, and dots. The second and important difference comes from the evaluation procedure, in which every characteristic of ABCD Rule has an associated score and a weight factor. When one evaluates a lesion, a characteristic score and the corresponding weight factor is multiplied to get an individual score for that characteristic. All four individual scores are finally summed for a resulting overall score for that lesion. If below 4.75, then the lesion is considered to be normal, if between 4.75 and 5.45, it is excised or followed up for some time period. If the score is above the threshold 5.45, then the lesion needs to be removed. Details about these four characteristics, their scores, and weight factor values are listed in Table 4.

2.2.3. Menzies scoring

Menzies Scoring partitions some of the features of a lesion into two groups. The first is the negative features group containing only two items: *symmetry* and *single color*. The second is the positive features group including nine items, listed in Table 5. The positive features are clear indicators of melanoma. Hence, if a lesion has none of the features in the negative group but a least one in the positive group, it is considered a melanoma case.

2.2.4. 7-Point Checklist

7-point Checklist is yet another method used for evaluating lesions by dermatologists in the second step (Malvehy et al., 2007). In this checklist, there are seven different features, whose combinations may indicate melanoma for a lesion. Every feature is assigned with a score (similar to ABCD Rule) and an overall score for the analyzed lesion is calculated depending on the existence of these specific features (see details in Table 6). If this overall score is greater than 3, melanoma is suspected. Fig. 6 further illustrates two melanoma cases which are evaluated according to 7-point Checklist with the detected features and the associated scores.

2.2.5. Comparative performance analysis of second step algorithms

Dolianitis et al. (2005) perform an experiment aiming at evaluating the performance of four aforementioned methods in the second step of visual inspection. In this experiment, 61 Australian medical practitioners are first trained in Pattern Analysis Criteria, ABCD Rule, Menzies Scoring and 7-Point Checklist algorithms, and later they assessed 40 images of melanocytic lesions. The statistical results of this experiment are reported in Table 7 in terms of sensitivity, specificity, and accuracy. Sensitivity here is the rate between the number of true positives, and the total number of true positives and false negatives, i.e., true positive rate. It simply refers to the rate of the correct classification of an individual as "melanoma" among all melanoma cases (Parikh et al., 2008). Specificity, on the other hand, refers to the rate between the number of true negatives, and the total number of true negatives and false

Table 2
First step "to-look-for-features" in the visual inspection. The suspected lesions are then evaluated by the second step. (There are minor exceptions to this table, see Malvehy et al., 2007.)

Dermoscopic criterion	Definition	Diagnostic Significance
Pigment Network-Pseudo-Network	Network of brownish interconnected lines overlying background of tan diffuse pigmentation. In facial skin a peculiar pigment network, also called pseudo-network, is typified by round, equally sized network holes corresponding to preexisting follicular ostia.	Melanocytic lesion
Aggregated globules	Numerous, variously sized, often clustered, round to oval structures with various shades of brown and gray-black. Should be differentiated from multiple blue-gray globules.	Melanocytic lesion
Streaks	These have been previously described separately as pseudopods and radial streaming, but are now combined into one term. They are bulbous and often kinked or finger-like projections seen at the edge of a lesion. They may arise from network structures but more commonly not.	Melanocytic lesion
Homogeneous blue pigmentation	Structureless blue pigmentation in absence of pigment network or other discernible structures.	Melanocytic lesion
Parallel pattern	Seen in melanocytic lesions of palms/soles and mucosal areas. On palms/soles pigmentation may follow sulci or cristae (ie, furrows or ridges) of the dermatoglyphics. Rarely arranged at right angles to these structures.	Melanocytic lesion
Multiple milia-like cysts	Numerous, variously sized, white or yellowish, roundish structures.	Seborrheic keratosis
Comedo-like openings	Brown-yellowish to brown-black, round to oval, sharply circumscribed keratotic plugs in the ostia of hair follicles. Irregularly shaped comedo-like openings are also called irregular crypts.	Seborrheic keratosis
Light brown fingerprint-like structures	Light brown, delicate, network-like structures with fingerprint pattern.	Seborrheic keratosis
Cerebriform pattern	Dark brown furrows between ridges producing brain-like appearance.	Seborrheic keratosis
Arborizing vessels	Tree-like branching telangiectases.	Basal cell carcinoma
Leaf-like structures	Brown to gray/blue discrete bulbous structures forming leaf-like patterns. They are discrete pigmented nests (islands) never arising from pigment network and usually not arising from adjacent confluent pigmented areas.	Basal cell carcinoma
Large blue-gray ovoid nests	Well-circumscribed, confluent or near confluent pigmented ovoid or elongated areas, larger than globules, and not intimately connected to pigmented tumor body.	Basal cell carcinoma
Multiple blue-gray globules	Multiple globules (not dots) that should be differentiated from multiple blue-gray dots (melanophages).	Basal cell carcinoma
Spoke-wheel areas	Well-circumscribed, radial projections, usually tan but sometimes blue or gray, meeting at often darker (dark brown, black, or blue) central axis.	Basal cell carcinoma
Ulceration	Absence of epidermis often associated with congealed blood, not due to well-described recent history of trauma.	Basal cell carcinoma
Red-blue lacunae	More or less sharply demarcated, roundish or oval areas with reddish, red-bluish, or dark-red to black.	Vascular lesion
Red-bluish to reddish-black homogeneous areas	Structureless homogeneous red-bluish to red-black areas.	Vascular lesion
None of listed criteria	Absence of above-mentioned criteria.	Melanocytic lesion

positives, i.e., true negative rate. It simply refers to the rate of correctly classifying an individual as "non-melanoma" among all non-melanoma cases. In short, if the system sensitivity and specificity values are high, the classification is almost certain that a test lesion has melanoma or not. From Table 7, Menzies Scoring has the highest sensitivity and accuracy, whereas the best specificity comes from Pattern Analysis Criteria. Since it is extremely important to identify both melanoma and non-melanoma cases, both Menzies Scoring and Pattern Analysis Criteria should be utilized.

2.3. Stage 3 — Feature generation, selection, and classification

As a last main stage, with the local and global features gathered in the previous two stages, namely lesion and feature segmentation, a classification procedure is applied. This stage starts with generating features of the lesion with the border information obtained from lesion segmentation, and with the feature masks obtained from feature segmentation. Generated features are all put together for every sample, and they are used as inputs for a classifier. Artificial Neural Networks (ANN) (Priddy and Keller, 2005), Support Vector Machines (SVMs) (Steinwart and Christmann, 2008), logistic regression (Tenenhaus et al., 2010), decision trees (Zhou and Song, 2013) and Bayesian classifiers (Li et al., 2014) are the most commonly used classifier types in this stage. Note here that, due to the great number and range of types of features that are possible, an optional feature selection (or dimensionality reduction) step can be allocated in the system in order to decrease the computational complexity.

In a methodological approach proposed by Celebi et al. (2007), after lesion segmentation, they extract shape features of the lesion border and

Table 3
Pattern Analysis Criteria features and definitions.

Global Features	Definition	Diagnostic significance
Reticular pattern	Pigment network covering most parts of the lesion.	Melanocytic nevus
Globular pattern	Numerous, variously sized, round to oval structures with various shades of brown and gray-black	Melanocytic nevus
Cobblestone pattern	Large, closely aggregated, somehow angulated globule-like structures resembling a cobblestone.	Dermal nevus
Homogeneous pattern	Diffuse, brown, gray-blue to gray-black pigmentation in the absence of other distinctive local features.	Melanocytic (blue) nevus
Starburst pattern	Pigmented streaks in a radial arrangement at edge of lesion.	Spitz/Reed nevus
Parallel pattern	Pigmentation on palms/soles that follows sulci or cristae (furrows or ridges), occasionally arranged at right angles to these structures.	Acral nevus/melanoma
Multicomponent pattern	Combination of >= 3 above-listed patterns.	Melanoma
Nonspecific pattern	Pigmented lesion lacking above patterns.	Possible melanoma
Local Features	**Definition**	**Diagnostic significance**
Pigment Network	Typical pigment network: light to dark brown network with small, uniformly spaced network holes and thin network lines distributed more or less regularly throughout lesion and usually thinning out at periphery. Atypical pigment network: black, brown, or gray network with irregular holes and thick lines.	Benign melanocytic lesion Melanoma
Dots/globules	Black, brown, round to oval, variously sized structures regularly or irregularly distributed within lesion.	If regular, benign melanocytic lesion If irregular, melanoma
Streaks (pseudopods and radial streaming)	Streaks are bulbous and often kinked or finger-like projections seen at the edge of lesion. They may arise from network structures but more commonly not. They range in color from tan to black.	If regular, benign melanocytic lesion (Spitz/Reed nevus) If irregular, melanoma
Blue-whitish veil	Irregular, structureless area of confluent blue pigmentation with an overlying white "ground-glass" film. Pigmentation cannot occupy entire lesion and usually corresponds to a clinically elevated part of the lesion.	Melanoma
Regression structures	White scar-like depigmentation and/or blue pepper-like granules usually corresponding to a clinically flat part of the lesion.	Melanoma
Hypopigmented areas (structureless/ homogeneous)	Focal areas devoid of structures with less pigmentation than overall pigmentation of lesion and comprising at least 10% of total area.	Nonspecific
Blotches	Black, dark brown, and/or gray structureless areas with symmetric or asymmetric distribution within lesion.	If symmetric, benign melanocytic lesion If asymmetric, melanoma
Vascular structures	Comma-like vessels. Hairpin vessels. Dotted vessels. Linear-irregular vessels. Vessels and/or erythema within regression structures.	Dermal nevus If uniformly distributed, seborrheic keratosis If irregularly distributed consider melanoma Melanoma Melanoma Melanoma

Table 4
ABCD Rule features, definitions, scores, and their weight factors.

Dermoscopic Criterion	Definition	Score	Weight Factor
A: Asymmetry	In 0, 1, or 2 perpendicular axes; assess not only contour, but also colors and structures.	0–2	1.3
B: Border	Abrupt ending of pigment pattern at periphery in 0-8 segments.	0–8	0.1
C: Color	Presence of up to 6 colors (white, red, light-brown, dark-brown, blue-gray, black).	1–6	0.5
D: Dermoscopic structures	Presence of network, structureless (homogeneous) areas, branched streaks, dots, and globules.	1–5	0.5

divide the lesion region into several possible clinical feature areas with the Euclidean Distance Transform. They utilize various feature selection algorithms to obtain most relevant, efficient, and effective features for classification, such as ReliefF (Kononenkoand and Simec, 1995), mutual information based feature selection (Battiti, 1994) and correlation based feature selection (Hall, 2000). They use an SVMs classifier, in which a grid search is carried out for the hyper-parameters of the radial basis kernel to obtain the optimal values (Sci-Kit Learn, 2017). Experiments on this system are evaluated with a set of 564 dermoscopic images, and resulted in 92.34% specificity and 93.33% sensitivity. Different approaches using a variety of available data produced thought-provoking results in this domain of research. For instance, Ganster et al.

Table 5
Menzies Scoring positive and negative features, and definitions.

Negative Features	Definition
Symmetry of pattern	Symmetry of pattern is required across all axes through lesion's center of gravity (center of lesion). Symmetry of pattern does not require shape symmetry.
Presence of a single color	The colors scored are black, gray, blue, dark brown, tan, and red. White is not scored as a color.
Positive Features	**Definition**
Blue-white veil	An area of irregular, structureless confluent blue pigmentation with an overlying white "ground-glass" haze. It cannot occupy entire lesion and cannot be associated with red-blue lacunae.
Multiple brown dots	Focal areas of multiple brown (usually dark brown) dots (not globules).
Pseudopods	Bulbous and often kinked projections that are found at the edge of lesion either directly connected to the tumor body or pigmented network. They can never be seen distributed regularly or symmetrically around the lesion. When connected directly to the tumor body, they must have an acute angle to the tumor edge or arise from linear or curvilinear extensions. When connected to the network, the width of the bulbous ending must be greater than the width of any part of the surrounding network and at least double that of its directly connected network projection.
Radial streaming	Finger-like extensions at the edge of lesion that are never distributed regularly or symmetrically around the lesion.
Scar-like depigmentation	Areas of white distinct irregular extensions (true scarring), which should not be confused with hypopigmentation or depigmentation due to simple loss of melanin.
Peripheral black dots/globules	Black dots/globules found at or near edge of lesion.
Multiple (5 or 6) colors	The colors scored are black, gray, blue, dark brown, tan, and red. White is not scored as a color.
Multiple blue/gray dots	Foci of multiple blue or gray dots (not globules) often described as "pepper-like" granules in pattern.
Broadened network	Network made up of irregular thicker "cords" of the net, often seen focally thicker.

Table 6
7-point Checklist features, definitions, and their scores.

Dermoscopic criterion	Definition	Score
1. Atypical pigment network	Black, brown, or gray network with irregular holes and thick lines.	2
2. Blue-whitish veil	Irregular, structureless area of confluent blue pigmentation with and overlying white "ground-glass" film. The pigmentation cannot occupy the entire lesion and usually corresponds to a clinically elevated part of the lesion.	2
3. Atypical vascular pattern	Linear-irregular or dotted vessels not clearly seen within regression structures	2
4. Irregular streaks	Brown to black, bulbous or finger-like projections irregularly distributed at the edge of lesion. They may arise from network structures but more commonly not.	1
5. Irregular dots/globules	Black, brown, round to oval, variously sized structures irregularly distributed within lesion.	1
6. Irregular blotches	Black, brown, and/or gray structureless areas asymmetrically distributed within lesion.	1
7. Regression structures	White scar-like depigmentation and/or blue pepper-like granules usually corresponding to clinically flat part of the lesion.	1

(2001) develop a K Nearest-Neighbor based algorithm using only shape and color features. The aim of their system is to classify these detected and extracted features into three classes, namely benign, dysplastic, and malignant. In the evaluation part, 5393 daily clinical lesion images are used as a dataset. A total of 122 features are gathered, extracted, and then reduced to 21 using a feature selection process. The overall experimental results demonstrate 87% sensitivity and 93% specificity on the used dataset. In another study, Rubegni et al. (2002) train an ANN classifier on a dataset of 588 images including more than 200 melanoma cases. They generate 48 features, grouped into four different categories:

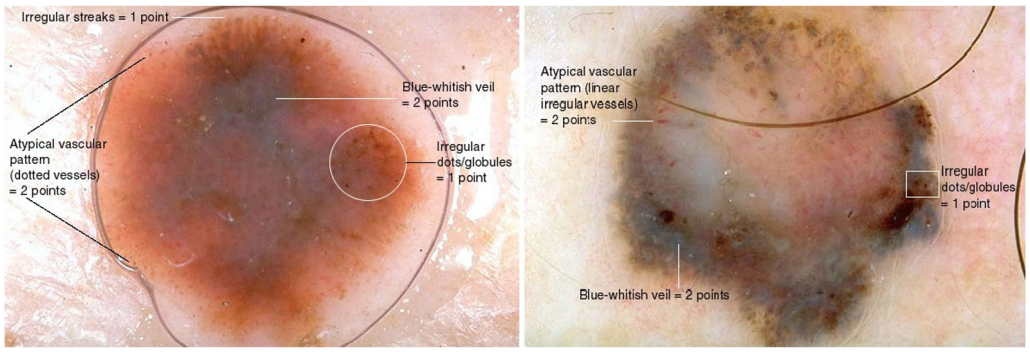

Fig. 6. Two cases of melanoma evaluated by 7-point Checklist. Different features detected with their associated scores can be observed (Features, 2017c).

Table 7
Performance analysis of four methods in the second step of visual inspection (Dolianitis et al., 2005).

Method	Sensitivity	Specificity	Accuracy
Pattern Analysis Criteria	68.4%	85.3%	76.8%
ABCD Rule	77.5%	80.4%	79.0%
Menzies Scoring	84.6%	77.7%	81.1%
7-point Checklist	81.4%	73.0%	77.2%

shape, color, texture, and islands of colors. After the feature selection process, the remaining 13 features, divided into two groups (shape and color) achieve a diagnostic accuracy of 94% with the trained network.

While example studies mentioned above mainly utilize global feature groups, there are also approaches which include local features. Situ et al. (2008) propose a bag-of-features approach using image patches of the segmented lesion region. The patches of size 16×16 pixels are extracted from a regular grid placed on the lesion. Then they use wavelets and "Gabor-like" filters (Schmid, 2001) as descriptors for those patches. A set of 10 features is gathered from wavelets and 13 additional features from Gabor-like filters. These obtained features are finally classified via a Naive Bayes classifier and an SVMs classifier. Experimental evaluations are carried out for 100 epiluminescence microscopy skin-lesion images, of which 70 are benign and the remaining 30, melanoma. After several repetition of the same experiment, the average results show a diagnostic accuracy level up-to 82.21% over these 100 test images. Barata et al. (2014) has recently considered the problem of strategy selection for lesion classification in terms of both global and local features. They propose two different systems in which the first one extracts global features and classifies them, and the second one defines regular key-points on the lesion region and then extracts local features to be classified. In this method, texture and color are used as two groups of features. Texture features are extracted from gradient-amplitude and gradient-orientation histograms. Color features are obtained from 6 different color spaces using RGB, HSV, HSI, LAB, LUV, and Opponent Color Space (Opp) (Bratkova et al., 2009; Tkalcic and Tasic, 2003) where each color distribution is characterized by concatenating the three color-channel histograms in the respective color space. Fig. 7 depicts simple block diagrams of these two systems. The experimental results indicate that both local and global feature based systems have good results in terms of accuracy; however, local features perform slightly better in terms of classification cost. The basic idea of utilizing local features is clearly a result of the success of such features in other areas, such as image retrieval (Douik et al., 2016) and object recognition (Guo et al., 2014). As a result, local features for melanoma detection has recently gained popularity, although the overall success still depends on methods used at each stage.

3. Recent studies and future directions

Research on automated melanoma detection started almost 30 years ago but accelerated after the invention of dermoscopy. All above mentioned studies made valuable contributions to melanoma detection. However, it is almost impossible to compare them because of different datasets with images taken from various dermoscopic tools in different resolutions and with varying types of artifacts. This section is further devoted to the latest studies, providing some insight into the state-of-the-art approaches, and deriving possible future directions on this topic.

3.1. Skin lesion analysis towards melanoma detection

Today, this is a topic of interest with new events such as Skin Lesion Analysis Towards Melanoma Detection (SLATMD) (SLATMD, 2017d). This is a challenge event in the IEEE International Symposium on Biomedical Imaging (ISBI) (ISBI, 2017e). Every year in ISBI, different grand challenges are chosen, and several teams take part in melanoma detection competition. The first ISBI-SLATMD was held in 2016, in which 28 teams competed in lesion segmentation and 25 teams competed in classification. A public dataset is provided by the organization, based on the ISIC Archive with 900 images for training and 350 images for testing. In addition, ground-truth information is also supplied by the organization for independent evaluation. Fig. 8 illustrates top-ten results for the lesion segmentation stage and the classification stage in ISBI-SLATMD 2016. In this figure, abbreviated evaluation metrics can be listed as follows: accuracy (AC); dice's similarity coefficient (DI) (Dice, 1945); jaccard index (JA) (Real and Vargas, 1996); sensitivity (SE); specificity (SP); area under the curve (AUC) (Bradley, 1997); and average precision (AP) (Robertson, 2008). A better objective evaluation is expected to have higher values for every aforementioned metric. However, the lesion segmentation stage is evaluated according to JA metric only, and the "malignant versus benign" binary-classification stage is evaluated according to AP metric only.

Following the success in 2016, another SLATMD challenge was held in ISBI 2017 and completed in April, 2017. With 593 registrations and 46 finalized submissions, it is said to be the largest ever comparative study in this field (Codella et al., 0000). A larger training dataset is provided by the organization, with 2000 images (374 melanoma, 254 seborrheic keratosis, and 1372 nevus) with additional masks and information for specific stages of the challenge, and the testing set consists of 600 images without labels. The organization also provides participants a validation set for the evaluation of their framework, and the results from 600 test images are evaluated for a final ranking, using an online system. The challenge is in three parts: lesion segmentation, dermoscopic feature segmentation (detection), and disease classification. In the first (lesion segmentation) part, training images are provided to participants together with manually traced borders (by experts) as a binary mask. The main testing task in this part is to submit an automated prediction of the segmented lesion as a binary image, which is later ranked by the JA metric. In the dermoscopic feature segmentation part, participants are asked to automatically detect four clinical features as network, negative network, streaks, and milia-like cysts. In particular, superpixel masks are provided alongside with the original images for training; and the

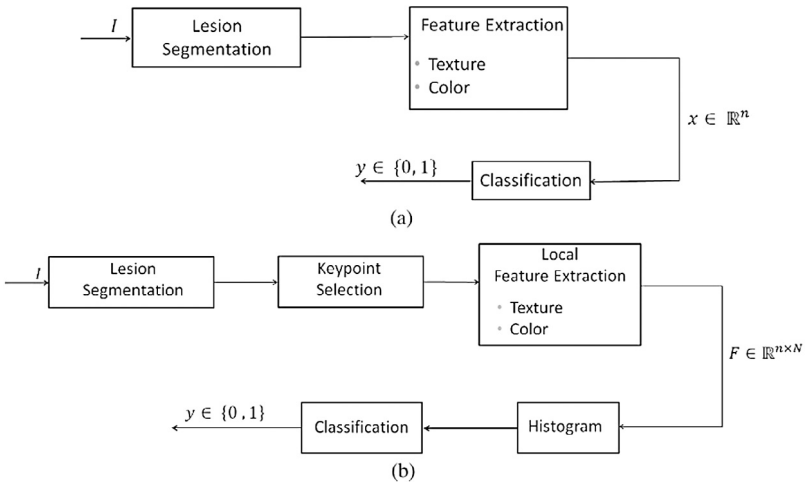

Fig. 7. Two melanoma detection systems proposed in Barata et al. (2014). (a) Classification with global features, and (b) classification with local features.

Method	AC	DI	JA	SE	SP
EXB	**0.953**	**0.910**	**0.843**	0.910	0.965
CUMED (ours)	0.949	0.897	0.829	0.911	0.957
Mahmudur	0.952	0.895	0.822	0.880	0.969
SFU-mial	0.944	0.885	0.811	**0.915**	0.955
TMUteam	0.946	0.888	0.810	0.832	**0.987**
UiT-Seg	0.939	0.881	0.806	0.863	0.974
IHPC-CS	0.938	0.879	0.799	0.910	0.941
UNIST	0.940	0.867	0.797	0.876	0.954
Jose Luis	0.934	0.869	0.791	0.870	0.978
Marco romelli	0.936	0.864	0.786	0.883	0.962

Method	AC	AUC	AP	SE	SP
CUMED	**0.855**	0.804	**0.637**	0.507	0.941
GTDL	0.813	0.802	0.619	0.573	0.872
BF-TB	0.834	**0.826**	0.598	0.320	0.961
ThrunLab	0.786	0.796	0.563	0.667	0.816
Jordan Yap	0.844	0.775	0.559	0.240	**0.993**
Haebeom Lee	0.821	0.793	0.555	0.200	0.974
GT-DL1	0.815	0.813	0.552	0.467	0.901
GT-DL2	0.681	0.800	0.545	0.787	0.655
Sebastien PARIS	0.731	0.793	0.542	0.773	0.720
USYD-BMIT	0.599	0.780	0.537	**0.853**	0.536

Fig. 8. Top-ten results in ISBI-SLATMD 2016 for (left) the lesion segmentation stage, and (right) the classification stage (Yu et al., 2017).

testing results are ranked by the AUC metric in this stage. In the final part, participants are asked to classify lesions as melanoma, seborrheic keratosis, or benign nevi. The additional data provided for this task includes the "gold standard" diagnosis, and age and gender information, if available. These test results are also ranked by AUC.

3.2. Recent studies

Convolutional Neural Networks (CNNs) (Smith and Topin, 0000) with their ability of hierarchical feature learning have great success in various (medical) image analysis problems, such as classification (Setio et al., 2016; Anthimopoulos et al., 2016), detection (Shin et al., 2016; Tajbakhsh et al., 2016), and segmentation (Ronneberger et al., 0000; Chen et al., 2017). In the ISBI-SLATMD 2016 challenge, the team named as CUMED who employ a very deep CNNs got the first place in the classification stage and the second place in the lesion segmentation stage (Yu et al., 2017). Their idea originates from the motivation that improved new training schemes along with very deep networks can achieve richer and more discriminative features. In this way, they basically try also to tackle a known "degradation problem" of training networks with increased number of layers. As the network goes deeper and deeper, its accuracy saturates and then degrades quickly. With a developed residual learning technique (ResNet) (He et al., 2016), the performance gain from the increasing number of layers can eventually be maintained. Hence, the proposed system architecture consists of two networks in which this newly developed residual learning is applied for both segmentation and classification stages (see Fig. 9). The first network is a fully convolutional residual network that segments the lesion region. In the training phase of this network, cropped ground-truth lesion (including close neighboring pixels) and non-lesion sub-images of each original dermoscopic image are collected, and all pixels in these rectangular areas are considered as training samples. In the testing phase, an input dermoscopic image as a whole is segmented, and a corresponding binary mask is produced as an output. The second network is a very deep residual network that classifies skin lesions based on the segmentation results. In the training phase of this network, automatically cropped lesion sub-images are resized to a fixed 250×250 pixels size. Two different classification networks are trained: the first uses a regular Softmax layer, and the second is placed with a linear SVMs layer (Tang, 2013). In the testing phase, the resized test lesion sub-image is classified using both classification networks, and the final result is the average of these two predictions. Experimental evaluations prove the success of CUMED, as already illustrated in Fig. 8.

The work of the CUMED team and their success is one of the most recent examples of CNNs for automated melanoma detection. Earlier works which influence the (very) deep CNNs concept include some approaches such that Kawaraha et al. (2016) and Codella et al. (2015). Kawaraha et al. (2016) propose a CNNs based framework where natural image features are utilized as convolutional filters. They use the Dermofit Image Library (Dermofit Image Library, 2017f) which includes 1300 non-dermoscopic skin images with the segmented ground-truth lesions and the corresponding classification labels. The main aim of their system is to avoid lesion segmentation, which is generally subjective, and to avoid complex pre/post-processing, which can also propagate errors. Therefore, CNNs as state-of-the-art feature extractors are fed directly with the original skin images, and pre-trained CNNs are employed for feature extraction to reduce the complexity. The used architecture AlexNet (Krizhevsky et al., 2012) is trained on natural images of ImageNet (Russakovsky et al., 2015). In addition, AlexNet CNNs are converted into full-CNNs by applying a similar approach to (Sermanet et al., 0000) in order to be able to extract features in multiple scales. Finally, a logistic regression classifier is used to classify these extracted multi-scale features. Experimental evaluation illustrates higher accuracies than previously reported results on the same dataset. In another study, Codella et al. (2015) propose a system where CNNs are combined with *sparse and redundant representations* (Elad, 2010) and SVMs. In this study, 2624 ISIC Archive images which contain 334 melanoma, 144 atypical nevi (looks like melanoma but it is not),

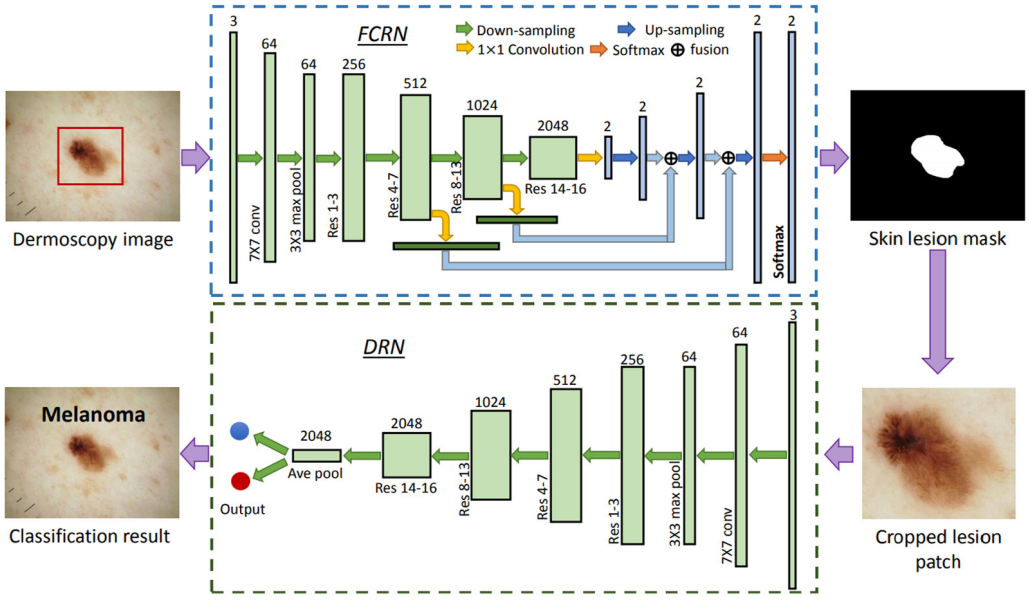

Fig. 9. The system architecture of CUMED team in the ISBI-SLATMD 2016 challenge. Residual networks are used for lesion segmentation and classification (Yu et al., 2017).

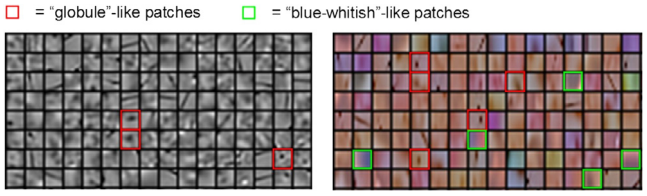

Fig. 10. Gray-scale and RGB dictionary subsets learned from the dataset. Some of the described clinical features can easily be identified, such as globules and blue-whitish structures (Codella et al., 2015).

and 2146 benign lesions are processed and evaluated. This dataset is thought to be difficult (even for experts), in which an"easier" task is first defined, to distinguish melanoma from other cases (i.e., atypical and benign), and then a "harder" one, to distinguish melanoma from atypical nevi. The proposed method consists mainly of two parallel paths. The first path includes CNNs (Caffé (Jia et al., 2014)) which are pre-trained on the natural photographs domain from Image Net (2017). The second path consists of two sparse representation dictionaries (for gray-scale and RGB color space) that are learned from the given dataset using dictionary learning algorithms in SPAMS (2017g), see Fig. 10. Both paths lead to a non-linear SVMs using a histogram intersection kernel (Maji et al., 2008) and sigmoid feature normalization. At the end, a fusion is done by unweighted SVMs score averaging.

In ISBI-SLATMD 2017, the most recent techniques competed and continued to improve the success in the area. Yuan et al. (0000) claim the first place in the lesion segmentation part of the challenge. After a pre-processing step in which all images are resized to a fixed 192 × 256 pixels size, they develop a framework based on "deep fully convolutional–deconvolutional neural networks" (CDNNs) (Noh et al., 2015) using HSV, LAB (L channel only), and RGB color spaces. They employ two types of image augmentation in order to improve the proposed system for various image acquisition conditions. The first augmentation consists in geometric transformations such as randomly flipping, rotating, shifting, and scaling, while the second type randomly normalizes the contrast of each color channel in every training image. The network architecture has a fixed stride, each convolutional–deconvolutional layer utilizes Rectified Linear Units (ReLUs), whereas the output layer uses a sigmoid, as the activation function. They train a 29-layer CDNNs using Adam optimization (Kingma and Ba, 0000), and the network basically outputs a pixel-based map indicating the probability that each input pixel belongs to the tumor region. Then a post-processing method with dual-thresholds (i.e., thresholding with high and low thresholds) followed by morphological dilation is applied to the CDNNs output to determine the tumor center and its region for the final binary tumor mask. By combining such outputs of an ensemble of 6 CDNNs, they achieve an average JA of 0.765, AC of 93.4%, and DI of 0.849 in lesion segmentation (Codella et al., 0000).

Automated dermoscopic feature detection (clinical feature segmentation) is the second part in the ISBI-SLATMD 2017 challenge. This part seems eventually to have the least information available, and the scarcity can be observed from the number of participations with only 3 submissions from 2 groups (Codella et al., 0000). The best performing approach for this task is from Kawahara and Hamarneh (0000). They reformulate the superpixel classification task as an image segmentation problem. While cleverly capturing spatial dependencies between superpixels, they first convert superpixels into segmentations; and later, transform the predicted segmentation masks obtained from the CNNs back into superpixels for labeling (see Fig. 11). They utilize an existing CNNs architecture (VGG16 Simonyan and Zisserman, 2015 pre-trained on ImageNet), and modify it to detect pixel-based dermoscopic features rather than classifying images. The modification is mainly related to the removal of fully connected layers, and the concatenation of feature maps from different layers in the network. The modified network is trained over 1700 images (from the challenge) to minimize a smoothed F1-score. The remaining 300 images are used for hyperparameter fine-tuning. As a result, they achieve an average AUC of 0.895 across all four dermoscopic feature classes, and win first place in the challenge.

"Lesion Feature Network" (LFN) of Li and Shen (0000) is ranked in the second place in the dermoscopic feature detection task. Yet another CNNs approach, it has 4 sequential stages and a total of 12 convolutional layers for feature extraction, as illustrated in the architecture in Fig. 12. The training images from the challenge are first subdivided into superpixels using the SLIC algorithm (Achanta et al., 2012) (e.g., Fig. 13), and then the extracted content of each superpixel is resized to a fixed size of 56 × 56 pixels. Later, a data augmentation is applied since the extracted patch dataset is severely imbalanced because of excessive amounts of background and pigment network patches. Here, they adopt random sampling for background and pigment network patches, and patch rotation with 90, 180, and 270 degrees for the remaining patches

Table 8
Disease classification task results in ISBI-SLATMD 2017 (Codella et al., 0000).

Method	AVG - AUC	M - AUC	SK - AUC
(Matsunaga et al., 0000) Top AVG classification (winner)	0.911	0.868	0.953
(Gonzalez-Diaz, 0000) Top SK classification	0.910	0.856	0.965
(Menegola et al., 2017b) Top M classification	0.908	0.874	0.943

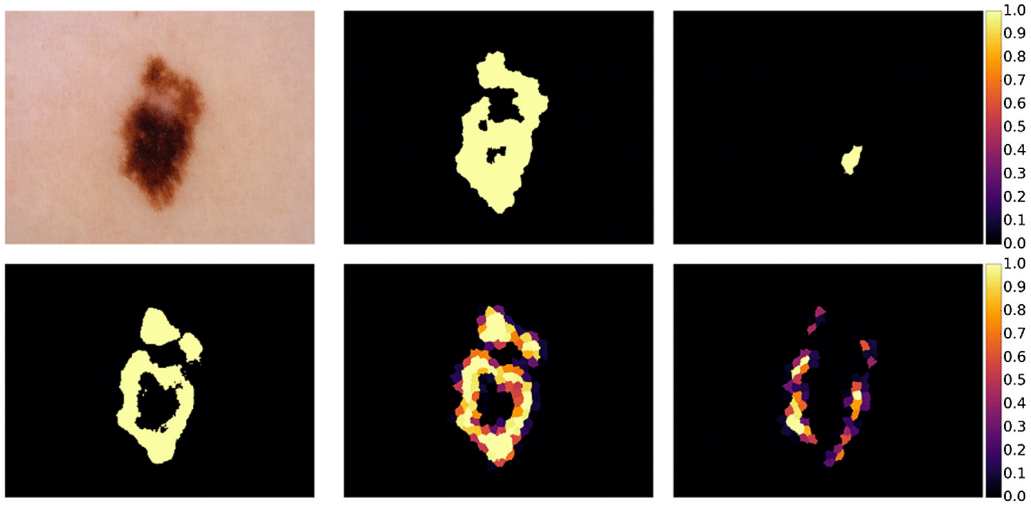

Fig. 11. (Top-left) The original image, and (middle) pigment network and (right) streaks converted into binary segmentations from superpixels. (Bottom-left) Pigment network prediction of the CNNs in Kawahara and Hamarneh (0000), and (middle) pigment network and (right) streaks converted into superpixels from segmentations (Kawahara and Hamarneh, 0000).

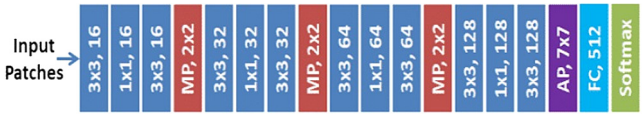

Fig. 12. Lesion Feature Network (Li and Shen, 0000). Blue blocks represent convolutional layers with kernel size and number of kernels. FC is the fully connected layer. Both max pooling (MP) and average pooling (AP) are utilized. (For interpretation of the references to colour in this figure legend, the reader is referred to the web version of this article.)

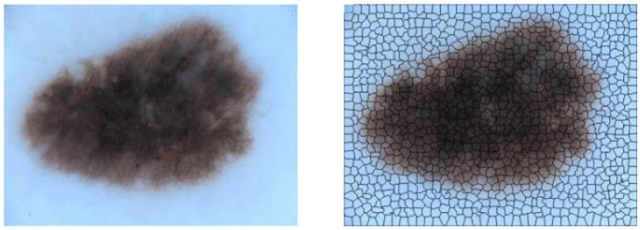

Fig. 13. (a) An example original skin lesion is (b) divided into superpixel areas (Li and Shen, 0000).

in order to balance the volumes of different categories. Finally, they train their network using the augmented patch dataset while assigning different weights for every class in the Softmax layer in order for further balancing the training among different classes. They achieve their best score with an average AUC of 0.833 after trying different versions of LFN (i.e., Narrow LFN and Wide LFN), please refer to Li and Shen (0000) for more information.

In the last part of ISBI-SLATMD 2017, 23 final test set submissions competed with each other for the disease classification task. The performance of success is analyzed according to the AUC score for melanoma (M) classification, seborrheic keratosis (SK) classification, and average (AVG) classification between two classes. Three winners of the challenge are listed in Table 8. Since seborrheic keratosis is a skin growth which is relatively hard to distinguish from melanoma, these three state-of-the-art techniques have indeed significant success in the area and will be explained in detail.

The AVG classification winner is the work from Matsunaga et al. (0000). They adopt 50-layer ResNet (ResNet-50) with small modifications. There are two base binary-classifiers in their system architecture, as illustrated in Fig. 14; the first one is trained for seborrheic keratosis versus rest (SK classifier), and the other one is trained for malignant melanoma versus rest (MM classifier). They extend the provided training dataset with an additional subset from the ISIC Archive. Before these training images and their geometric transformations are fed into the base classifiers in an ensemble of pre-trained CNNs, a normalization of luminance and color balance is performed using color constancy (Barata et al., 2015). Their system also considers the provided age/sex information, by applying a simple thresholding, based on the fact that "*SK and MM are rare at young ages in general*". However, this feature is included only for SK while noting that there is no significant improvement for MM classification. Another aspect of this system is that the SK classification information is integrated into the MM classification, by formulating a linear approximation which supports the notion of "*if a sample is very likely to be SK, it probably won't be MM*" (Matsunaga et al., 0000). Furthermore, they also trained their system using the training dataset from ISBI-SLATMD 2016 and some additional samples from the ISIC Archive, and eventually achieve an average AUC of 0.874 and AP of 0.744 which outperforms the aforementioned team CUMED.

The best SK classification result in ISBI-SLATMD 2017 is from the approach of Gonzalez-Diaz (Gonzalez-Diaz, 0000), which incorporates the expert knowledge from dermatologists into CNNs. Their system design includes several networks and it follows a four-step pipeline as demonstrated in Fig. 15. First, the input image is fed into a "lesion segmentation net", which is a fully convolutional network (FCN) (Shelhamer et al., 0000) trained on the provided dataset for the lesion segmentation task in the challenge. The output is simply a binary mask outlining the lesion area. Next, the original image and its lesion

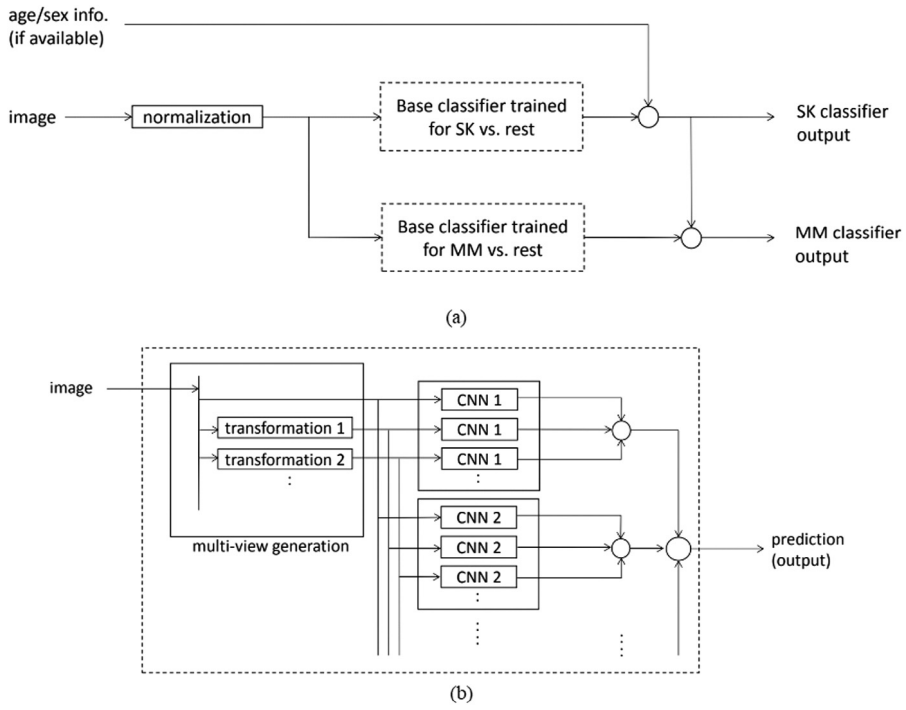

Fig. 14. (a) System architecture, and (b) base classifiers from Matsunaga et al. (0000).

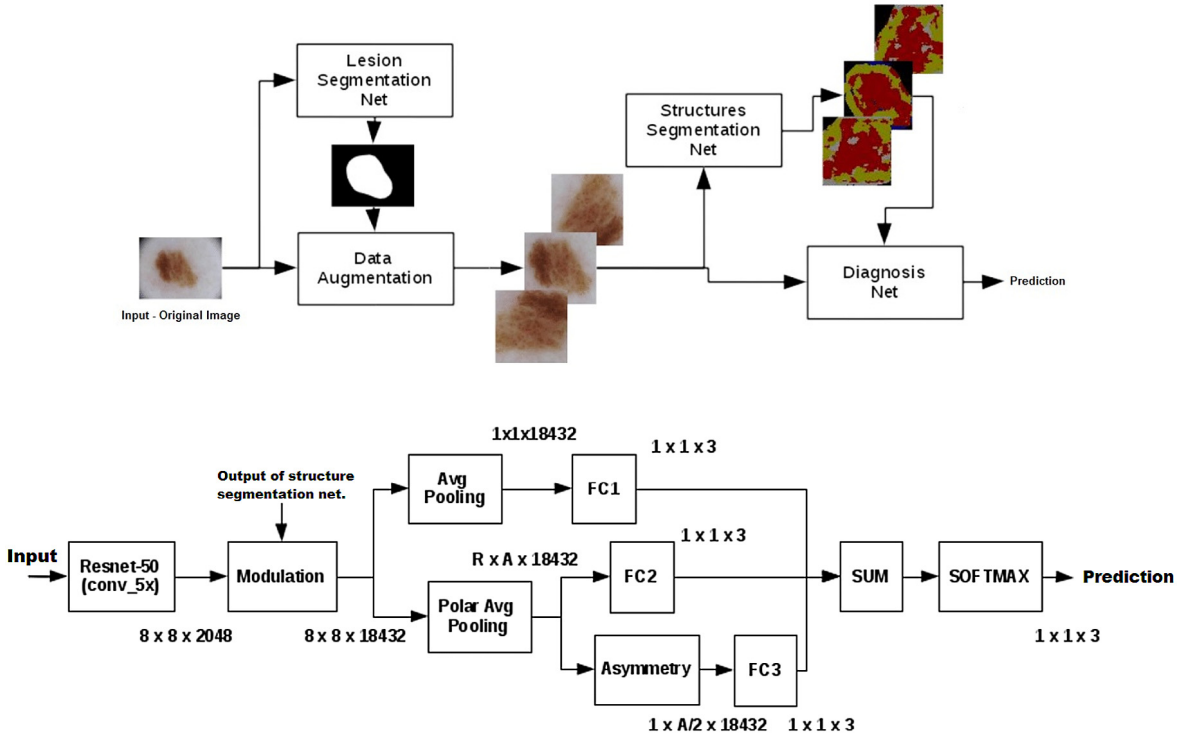

Fig. 15. (Top) General processing pipeline, and (bottom) the "diagnosis net" of Gonzalez-Diaz (0000).

mask as a pair goes into the "data augmentation" module, in which an augmented set of 24 images is generated through rotation, resizing, and cropping operations on the input pair. In addition, normalized polar coordinates are computed from each lesion mask in order to provide the system invariance against shifts, rotations, size changes, and shape irregularities of lesions. "Structures segmentation net" aims at segmenting eight important local and global dermoscopic features, i.e., dots, globules, and cobblestone pattern; reticular patterns and pigmented networks; homogeneous areas; regression areas; blue-white veil; streaks; vascular structures; and unspecific patterns. To do so, dermatologists from a collaborating medical institution weakly-annotated the training dataset of ISBI-SLATMD 2016 with the local or global presence, or absence of these considered structures. This network is a modified version of Simonyan and Zisserman (2015) with an additional

constrained optimization with these weak annotations (Pathak et al., 2015), and it outputs a probability map for each considered structure. Lastly, a final clinical diagnosis is provided by the "diagnosis net" by gathering all information extracted from previous modules. This network is yet another modified version of the ResNet-50 which has three novel units as can been seen in Fig. 15. In short, the "modulation" block merges the structure segmentation maps with the output of ResNet-50. "Polar pooling" is technically a pooling layer, but (normalized) polar coordinate sectors are processed instead of rectangular spatial regions. The "asymmetry" block evaluates the asymmetry of a lesion for a given angle based on the previous polar pooling. Together with three fully connected layers in Fig. 15, the results in each branch are linearly combined to produce a final output.

The top M classification result is obtained by the team RECOD Titans (Menegola et al., 2017b). They basically attack three issues regarding to the performance of deep learning methods: volume of the training data, depth of the model, and availability of the computational power. In terms of the data volume, they combine six sources from ISBI-SLATMD 2017 challenge, ISIC Archive, EDRA, PH2, Dermofit Library, and IRMA Skin Lesion Dataset (unlisted, available under request) and produce two subsets, namely, *deploy* with 9640 images and *semi* with 7544 images. Their approach for the network model is inspired from their previous experience (Menegola et al., 2017a) in which a pre-trained network on ImageNet tailored by fine-tuning for lesion classification. Hence, they select (deeper) ResNet-101 and Inception-v4 (Szegedy et al., 0000) as basis and then evaluate hundreds of models through these networks. In the end, they have a meta-model including seven base models: three based on Inception trained on deploy; three based on Inception trained on semi; and one based on ResNet trained on 'semi; and a SVMs based meta-learning layer trained on the validation set of deploy. The team argues that their success originates from the deeper models with larger datasets, data augmentation methods, per-image normalization (e.g., subtracting the image average boosts Inception), and fusion of the decisions from different models (i.e., leads to better results than a single best model).

3.3. Melanoma detection with smart phones

With the current technological advancements, smart phones are equipped with relatively powerful processors and high-definition cameras. This fact naturally gives a chance to detect/predict melanoma through non-dermoscopic images captured with smart phones, which may pave the way for increasingly number of mobile applications (apps) in dermatology (Brewer et al., 2013; Patel et al., 2014). However, there are studies stating that mobile applications may indeed produce a potential danger for users in terms of questions over diagnosis accuracy and reliability, hence may delay the diagnosis of melanoma (Wolf et al., 2013). Another point is that a correct assessment of a mobile application is very difficult due to scarcity and misinformation. For example in Kassianos et al. (2015), 39 mobile applications for melanoma detection are investigated. Although some these applications provide useful information and education about melanoma, ultraviolet radiation, and skin examination strategies, the statistics show that almost a quarter send the captured images to an expert dermatologist for an evaluation result. There are some applications relying only on the comparison of images, which require taking series of images in time. In addition, seven of these investigated applications have limited information on the processing of images. Moreover, there are applications which have not been updated over several years, or lack proper documentation even if updated recently. Unfortunately, none of these investigated applications seems to get validated for diagnostic accuracy or established in scientific research. Therefore, mobile applications for melanoma detection need further validation for their accuracy and reliability. As a final note, there is a recent commentary related to these issues in Vang et al. (2017).

3.4. Possible future directions

Automated melanoma detection can basically be thought of as a two-step classification problem. In a given dermoscopic image, the first step aims at classifying pixels or pixel groups into lesion and non-lesion clusters. The second step then consists of segmenting and classifying the lesion-classified pixels or groups of pixels into melanoma or non-melanoma categories. From ISBI-SLATMD challenges and the proposed solutions to the problem, the trend seems evolving towards a two-step approach rather than the previously mentioned three-step pipeline. It appears that the clinical feature segmentation step is being omitted, or merged with the other two steps. The cause might be the technical framing of the ISBI-SLATMD organization or the comprehended importance of this task (Codella et al., 0000), or it can be simply due to the embedded feature extraction nature of state-of-the-art deep learning methods. Nevertheless, the best SK classification method in Gonzalez-Diaz (0000) includes all three stages implemented with CNNs and achieves a comparable (average) AUC of 0.856 for melanoma detection, see Table 8. It should be noted here that in addition to (Gonzalez-Diaz, 0000), the winner of the challenge in Matsunaga et al. (0000) and the top M classification in Menegola et al. (2017b) both utilize modified pre-trained CNNs models. To sum up here, ensembles of modified deep learning structures utilizing pre-trained models (especially on ImageNet) have led to the current state-of-the-art results.

One of the aspects that stands out regarding models is the dataset used for training. The trend moves to the direction of increasing the volume and variety of training data with different data augmentation methods, and even further, with external data sources which indeed seems to help obtain better performance. Another important point worth mentioning is that the fusion of several model outputs improves the overall success, e.g., (Menegola et al., 2017b). This is also proven in Codella et al. (0000) by employing three fusion strategies (i.e., score averaging, linear SVMs, non-linear SVMs) based on a similar work (Marchetti et al., 2018) in ISBI-SLATMD 2016. These strategies evaluate all final submissions on the final test set and calculate one fused score for a particular case. The best fusion method emerges as the "linear SVMs" which achieves results that outperform all other single systems. In general, re-purposing CNNs or ensembles of them with appropriate modifications and incorporating supporting mechanisms seem to be a useful direction for further improving the obtained success at the moment. The crucial question here is: "What else can be done to boost these results?"

To the best of our knowledge, few studies, as mentioned previously, deal with this problem in a sparse and redundant representations framework. Indeed, the nature of the problem means sparsity-related tools are very suitable. In detail, the bordering pixels (where a transition occurs from lesion to background) of a lesion are sparse in nature when compared to the pixel groups contained in the lesion region as well as in the background skin region. Similarly, clinical features located in the lesion region happen to be sparsely distributed when compared to the remaining pixels in the lesion. Hence, the lesion and clinical feature segmentation and classification problems could be deployed in a sparse representations optimization framework, which eventually might lead to better learned (multi-)models of melanoma detection.

Sparse representations basically represent most or all information contained in a signal with a weighted linear combination of a small number of elements or *atoms* taken from an overcomplete or redundant basis or *dictionary*. Such a dictionary is a set of atoms whose number is much larger than the dimension of the feature space. Any signal then admits an infinite number of representations, and the sparsest such solution has interesting aspects for various signal and image processing tasks, e.g., (Elad and Aharon, 2006; Protter and Elad, 2009; Peyre, 2009; Mairal et al., 2008a, b; Bryt and Elad, 2008; Peotta et al., 2006; Fadili et al., 2007; Mairal et al., 2008; Liao and Sapiro, 2008). In mathematical terms, a sparsity-constrained non-convex optimization is solved with two approximate convex optimization steps: (*i*) sparse coding, and (*ii*)

dictionary update; and a solution can be reached by iteratively solving these two steps. A wide variety of *greedy pursuit algorithms* for sparse coding and *dictionary update techniques* are introduced in literature with strong theoretical foundations and better performance evaluations in comparison to other signal and image processing tools (Elad, 2010). For more information, please refer to Elad (2010).

Sparse representations mainly implement a suitable data transformation which increases the dimensionality of feature space, and then can be searched for related subspaces (lesion/non-lesion and melanoma/non-melanoma) within this new high-dimensional feature space. Both feature transformation (i.e., sparse coding) and learned overcomplete dictionaries can also be enforced with the help of a "structure" constraint. Therefore, additional structural-pattern constraints can be employed, and then manipulated so that subspaces can directly be designated as clusters for classification. As one example, *group sparsity* (Meier et al., 2008; Friedman et al., 0000; Huang and Zhang, 2010; Huang et al., 2011) groups the elements of sparse-codes by allowing sparse coefficients to fill the representation vector group-by-group. *Block sparsity* (Eldar and Mishali, 2009; Elhamifar and Vidal, 2009) is yet a specific case of group sparsity in which only one of the groups is non-zero and all others are forced to be zero. Constraining block sparsity structure into sparse codes by the sparse coding step followed by a dictionary learning basically corresponds to learning a corresponding block-sparse model for the data where learned sub-dictionaries together with the supporting block of sparse codes define distinct subspaces which can later be utilized for classification purposes. It is very important here to keep in mind that structured sparsity is a sparse coding approach that will work particularly well if the data has that specific structural nature (Huang and Zhang, 2010). Hence, one possible research direction might be to implement and test the whole structured sparsity concept for the melanoma detection problem. Moreover, related to the block sparsity structure, *deep sparse structures* as proposed in Oktar and Turkan (2018) would be another rewarding aspect of sparsity-related concept, first in terms of its theoretical foundation, and then of practical application to automated melanoma detection.

4. Conclusions

Melanoma is a very dangerous skin cancer type. The danger originates from its ability to metastasize; fortunately, it is curable if identified in its early stages. Currently, there are publicly available guidelines as well as various public facilities and events for the assessment of skin surface lesions and moles. If a lesion is suspected to be malignant, a visual investigation needs to be performed by a dermatologist. Although melanoma can be identified visually by investigators, there is indeed a strong need for automated detection tools because of the subjectivity problem. The research on this subject is accelerated with the proliferation of dermoscopic tools, and the majority of successful works in literature perform the detection in a small number of consecutive steps, namely, lesion segmentation, clinical (feature) segmentation, and (disease/feature) classification.

Recent advancements show that deep learning and sparse representations based methods (or ensembles of them) will continue improving the success rate in this area of research. New ISBI-SLATMD challenges with publicly available large datasets will undoubtedly help in accelerating these state-of-the-art achievements. In the near future, it is also highly probable that it will be possible to accurately detect melanoma by means of a mobile device.

As a final point, it is very important to mention here that dermatology is unlikely to be sufficient to reach a fully successful automated melanoma detection system; observations of dermatologists clearly need to be supported with the diagnosis information from pathologists.

Acknowledgment

Authors are grateful to Prof. Dr. Ugur Pabuccuoglu for fruitful discussions about dermatology and pathology, and for his constructive comments that greatly improved the manuscript.

References

Abbas, Q., Garcia, I.F., Celebi, M.E., Ahmad, W., Mushtag, Q., 2013. A perceptually oriented method for contrast enhancement and segmentation of dermoscopy images. Skin Res. Technol. 19 (1), 490–497.

Achanta, R., Shaji, A., Smith, K., Lucchi, A., Fua, P., Susstrunk, S., 2012. SLIC superpixels compared to state-of-the-art superpixel methods. IEEE Trans. Pattern Anal. Mach. Intell. 34 (11), 2274–2282.

Airley, R., 2009. Cancer Chemotherapy: Basic Science to the Clinic. Wiley.

Akram, M.U., Tariq, A., Khalid, S., Javed, M.Y., Abbas, S., Yasin, U., 2015. Glaucoma detection using novel optic disc localization, hybrid feature set and classification techniques. Australasian Phys. Eng. Sci. Med. 38 (4), 643–655.

Anthimopoulos, M., Christodoulidis, S., Ebner, L., Christe, A., Mougiakakou, S., 2016. Lung pattern classification for interstitial lung diseases using a deep convolutional neural network. IEEE Trans. Med. Imag. 35 (5), 1207–1216.

Argenziano, G., Soyer, H.P., Chimenti, S., Talamini, R., Corona, R., Sera, F., Binder, M., Cerroni, L., Rosa, G.D., Ferrara, G., Hofmann-Wellenhof, R., 2003. Dermoscopy of pigmented skin lesions: results of a consensus meeting via the internet. J. Am. Acad. Dermatol. 48 (9), 679–693.

Argenziano, G., Soyer, H.P., Giorgio, V.D., Piccolo, D., Carli, P., Delfino, M., Ferrari, A., Hofmann-Wellenhof, R., Massi, D., Mazzocchetti, G., Scalvenzi, M., Wolf, I.H., 2000. Interactive Atlas of Dermoscopy. Milan: Edra Medical Publishing and New Media.

Bad.Org, 2017. ABCD - Easy guide to checking your moles. http://www.bad.org.uk/for-the-public/skin-cancer/melanoma-leaflets/abcd-easy-guide-to-checking-your-moles.(Accessed 4 July 2017).

Baral, B., Gonnade, S., Verma, T., 2014. Lesion segmentation in dermoscopic images using decision based neuro fuzzy model. IJCSIT 5 (2), 2546–2552.

Barata, C., Celebi, M.E., Marques, J.S., 2015. Improving dermoscopy image classification using color constancy. IEEE J. Biomed. Health Inf. 19 (3), 1146–1152.

Barata, C., Ruela, M., Francisco, M., Mendonca, T., Marques, J.S., 2014. Two systems for the detection of melanomas in dermoscopy images using texture and color features. IEEE Syst. J. 8 (3), 965–979.

Battiti, R., 1994. Using mutual information for selecting features in supervised neural net learning. IEEE Trans. Neural Netw. 5 (4), 537–550.

Bethesda Cancer, 2017. Skin cancer, case study. http://www.bethesdacancer.com/wp-content/uploads/2017/01/Skin-Cancer-Case-Study.pdf. (Accessed 13 September 2017).

Bradley, A., 1997. The use of the area under the roc curve in the evaluation of machine learning algorithms. Pattern Recognit. 30 (7), 1145–1159.

Bratkova, M., Boulos, S., Shirley, P., 2009. oRGB: A practical opponent color space for computer graphics. IEEE Comput. Graph. Appl. 29 (1), 42–55.

Braun, R.P., Rabinovitz, H.S., Oliviero, M., Kopf, A.W., Saurat, J.H., 2005a. Dermoscopy of pigmented skin lesions. J. Am. Acad. Dermatol. 52 (1), 109–121.

Braun, R.P., Rabinovitz, H.S., Oliviero, M., Kopf, A.W., Saurat, J.-H., 2005b. Dermoscopy of pigmented skin lesions. J. Am. Acad. Dermatol. 52 (1), 109–121.

Brewer, A., Endly, D.C., Henley, J., Amir, M., Sampson, B.P., Moreau, J.F., Dellavalle, R.P., 2013. Mobile applications in dermatology. JAMA Dermatol. 149 (11), 1300–1304.

Bryt, O., Elad, M., 2008. Compression of facial images using the K-SVD algorithm. J. Vis. Commun. Image Represent. 19 (4), 270–283.

Cancer.Org, 2017a. Key statistics for melanoma skin cancer. https://www.cancer.org/cancer/melanoma-skin-cancer/about/key-statistics.html. (Accessed 13 September 2017).

Cancer.Org, 2017b. Cancer facts and figures in USA. https://www.cancer.org/content/dam/cancer-org/research/cancer-facts-and-statistics/annual-cancer-facts-and-figures/2017/cancer-facts-and-figures-2017.pdf.(Accessed 4 July 2017).

Castillo, O., Melin, P., 2008. Type-2 Fuzzy Logic: Theory and Applications. Springer.

Celebi, M.E., Kingravi, H.A., Uddin, B., Iyatomi, H., Aslandogan, Y.A., Stoecker, W.V., Moss, R.H., 2007. A methodological approach to the classification of dermoscopy images. Comput. Med. Imaging Graph. 31 (1), 362–373.

Celebi, M.E., Schaefer, G., Iyatomi, H., Stoecker, W.V., 2009a. Lesion border detection in dermoscopy images. Comput. Med. Imaging Graph. 33 (2), 148–153.

Celebi, M.E., Schaefer, G., Iyatomi, H., Stoecker, W.V., Malters, J.M., Grichnik, J.M., 2009b. An improved objective evaluation measure for border detection in dermoscopy images. Skin Res. Technol. 15 (4), 444–450.

Celebi, M.E., Wen, Q., Hwang, S., Iyatomi, H., Schaefer, G., 2013. Lesion border detection in dermoscopy images using ensembles of thresholding methods. Skin Res. Technol. 19 (1), 252–258.

Chen, H., Qi, X., Yu, L., Dou, Q., Qin, J., Heng, P.-A., 2017. DCAN: Deep contour-aware networks for object instance segmentation from histology images. Med. Imag. Anal. 36, 135–146.

Codella, N., Cai, J., Abedini, M., Garnavi, R., Halpern, A., Smith, J.R., 2015. Deep learning, sparse coding, and SVM for melanoma recognition in dermoscopy images, in: Int. W. Mach. Learning Med. Imag., Vol. 9352, pp. 118–126.

Codella, N.C.F., Gutman, D., Celebi, M.E., Helba, B., Marchetti, M.A., Dusza, S.W., Kalloo, A., Liopyris, K., Mishra, N.K., Kittler, H., Halpern, A., 0000. Skin lesion analysis toward melanoma detection: A challenge at the 2017 International Symposium on Biomedical Imaging (ISBI), Hosted by the International Skin Imaging Collaboration (ISIC), CoRR arxiv.org/abs/1710.05006.

Day, G., Barbour, R., 2000. Automated melanoma diagnosis: Where are we at? Skin. Res. Tech. 6 (1), 1–5.

DermLite, 2017a. https://dermlite.com/. (Accessed 20 July 2017).
Dermofit Image Library, 2017b. https://licensing.eri.ed.ac.uk/i/software/dermofit-image-library.html. (Accessed 7 October 2017).
Dice, L.R., 1945. Measures of the amount of ecologic association between species. Ecology 26 (3), 297–302.
Dolianitis, C., Kelly, J., Wolfe, R., Simpson, P., 2005. Comparative performance of 4 dermoscopic algorithms by nonexperts for the diagnosis of melanocytic lesions. Arch. Dermatol. 141 (8), 1008–1014.
Douik, A., Abdellaoui, M., Kabbai, L., 2016. Content based image retrieval using local and global features descriptor, in: Int. Conf. Adv. Technol. Signal Image Process., pp. 151–154.
Elad, M., 2010. Sparse and Redundant Representations: From Theory To Applications in Signal and Image Processing. Springer.
Elad, M., Aharon, M., 2006. Image denoising via sparse and redundant representations over learned dictionaries. IEEE Trans. Image Process..
Eldar, Y.C., Mishali, M., 2009. Robust recovery of signals from a structured union of subspaces. IEEE Trans. Inform. Theory 55 (11), 5302–5316.
Elhamifar, E., Vidal, R., 2009. Sparse subspace clustering, in: IEEE Comp. Vis. Pattern Recog., pp. 2790–2797.
Ercal, F., Chawla, A., Stoecker, W.V., Lee, H.-C., Moss, R.H., 1994. Neural network diagnosis of malignant melanoma from color images. IEEE Trans. Biomed. Eng. 41 (9), 837–845.
EuroMelanoma.Org, 2017. Turkiye euromelanoma tarama merkezleri. http://www.euromelanoma.org/turkey. (Accessed 4 July 2017).
Fadili, M.J., Starck, J.L., Murtagh, F., 2007. Inpainting and zooming using sparse representations. Comput. J. 52 (1), 64–79.
Features, 2017c. http://www.dermoscopy.org/consensus/2d.asp. (Accessed 16 July 2017).
Friedman, J., Hastie, T., Tibshirani, R., 0000. A note on the group lasso and a sparse group lasso, arxiv.org/abs/1001.0736.
Ganster, H., Pinz, A., Roehrer, R., Wildling, E., Binder, M., Kittler, H., 2001. Automated melanoma recognition. IEEE Trans. Med. Imaging 20 (3), 233–239.
Garnavi, R., Aldeen, M., Celebi, M.E., Varigos, G., Finch, S., 2011. Border detection in dermoscopy images using hybrid thresholding on optimized color channels. Comput. Med. Imaging Graph. 35 (2), 105–115.
Gonzalez-Diaz, I., 0000. Incorporating the knowledge of dermatologists to convolutional neural networks for the diagnosis of skin lesions, CoRR arxiv.org/abs/1703.01976.
Guo, Y., Bennamoun, M., Sohel, F., Lu, M., Wan, J., 2014. 3D object recognition in cluttered scenes with local surface features: A survey. IEEE Trans. Pattern Anal. Mach. Intell. 36 (11), 2270–2287.
Hall, M.A., 2000. Correlation-based feature selection for discrete and numeric class machine learning, in: Int. Conf. Machine Learn., pp. 359–366.
Hayashi, A., Suematsu, N., Ishida, Y., Kanbara, T., 2005. Region-based image retrieval using wavelet transform. In: Digital Image Process. Springer.
He, K., Zhang, X., Ren, S., Sun, J., 2016. Deep residual learning for image recognition, in: IEEE Conf. Comp. Vis. Pattern Recog., pp. 770–778.
Huang, L.K., Wang, M.J.J., 1995. Image thresholding by minimizing the measures of fuzziness. Pattern Recognit. 28 (1), 41–51.
Huang, J., Zhang, T., 2010. The benefit of group sparsity. Annals Stat. 38 (4), 1978–2004.
Huang, J., Zhang, T., Metaxas, D., 2011. Learning with structured sparsity. J. Mach. Learn. Res. 12, 3371–3412.
IARC, 2017. Malignant melanoma of skin. http://eco.iarc.fr/eucan/Cancer.aspx?Cancer=20. (Accessed 13 September 2017).
Image Net, 2017. ImageNet Large Scale Visual Recognition Challenge, 2012. http://image-net.org/challenges/LSVRC/2012/. (Accessed 8 October 2017).
ISBI, 2017d. http://biomedicalimaging.org/2017/. (Accessed 19 July 2017).
ISIC, 2017e. ISIC Archive: The international skin imaging collaboration: Melanoma project. https://isic-archive.com/#. (Accessed 20 July 2017).
Iyatomi, H., Oka, H., Saito, M., Miyake, A., Kimoto, M., Yamagami, J., Kobayashi, S., Tanikawa, A., Hagiwara, M., Ogawa, K., Argenziano, G., Soyer, H.P., Tanaka, M., 2006. Quantitative assessment of tumour extraction from dermoscopy images and evaluation of computer-based extraction methods for an automatic melanoma diagnostic system. Melanoma Res. 16 (2), 183–190.
Jamil, U., Khalid, S., Akram, M.U., 2016. Dermoscopic feature analysis for melanoma recognition and prevention, in: Int. Conf. Inno. Comp. Technol., pp. 290–295.
Jia, Y., Shelhamer, E., Donahue, J., Karayev, S., Long, J., Girshick, R., Guadarrama, S., Darrell, T., 2014. Caffe: Convolutional architecture for fast feature embedding, in: ACM Int. Conf. Multimedia, pp. 675–678.
Kanser.Gov.Tr, 2017. Turk halk sagligi kurumu kanser daire baskanligi. http://kanser.gov.tr/kanser/kanser-turleri/48-melanoma.html. (Accessed 4 July 2017).
Kanser Vakfi, 2017. Turkiye kanserle savas vakfi. http://www.kanservakfi.com/melanom-cilt-kanseri-117.html. (Accessed 4 July 2017).
Kapur, J.N., Sahoo, P.K., Wong, A.K.C., 1985. A new method for gray-level picture thresholding using the entropy of the histogram. Comput. Vis. Graph. Image Process. 29 (1), 273–285.
Kassianos, A.P., Emery, J.D., Murchie, P., Walter, F.M., 2015. Smartphone applications for melanoma detection by community, patient and generalist clinician users: a review. British J. Dermatol. 172 (6), 1507–1518.
Katsambas, A., Lotti, T., Dessinioti, C., D'Erme, A.M., 2015. European Handbook of Dermatological Treatments. Springer.
Kawaraha, J., BenTaieb, A., Hamarneh, G., Deep features to classify skin lesions, in: IEEE Int. Symp. Biomed. Imag., pp. 1397–1400.
Kawahara, J., Hamarneh, G., 0000. Fully convolutional networks to detect clinical dermoscopic features, CoRR arxiv.org/abs/1703.04559.
Kingma, D.P., Ba, J., 0000. Adam: A method for stochastic optimization, CoRR arxiv.org/abs/1412.6980.
Kittler, J., Illingworth, J., 1986. Minimum error thresholding. Pattern Recognit. 19 (1), 41–47.
Kononenkoand, I., Simec, E., 1995. Induction of decision trees using relieff. In: W. Math. Stat. Methods in AI. pp. 199–220.
Krizhevsky, A., Sutskever, I., Hinton, G.E., 2012. Imagenet classification with deep convolutional neural networks, in: Int. Conf. Neural Info. Process. Syst., pp. 1097–1105.
Lee, K.T., 2001. Measuring Border Irregularity and Shape of Cutaneous Melanocytic Lesions (Ph.D thesis), Simon Fraser University, Canada.
Lee, T., Ng, V., Gallagher, R., Coldman, A., McLean, D., 1997. Dullrazor: A software approach to hair removal from images. Comput. Biol. Med. 27 (6), 533–543.
Li, Y., Shen, L., 0000. Skin lesion analysis towards melanoma detection using deep learning network, CoRR arxiv.org/abs/1703.00577.
Li, L., Zhang, Q., Ding, Y., Jiang, H., Thiers, B.H., Wang, Z.J., 2014. Automatic diagnosis of melanoma using machine learning methods on a spectroscopic system. BMC Med. Imag. 14 (1).
Liao, H.Y., Sapiro, G., 2008 .Sparse representations for limited data tomography, in: IEEE Int. Symp. Biomed. Imag., pp. 1375–1378.
Mairal, J., Bach, F., Ponce, J., Sapiro, G., Zisserman, A., 2008. Discriminative learned dictionaries for local image analysis, in: IEEE Comp. Vis. Pattern Recog., pp. 1–8.
Mairal, J., Elad, M., Sapiro, G., 2008a. Sparse representation for color image restoration. IEEE Trans. Image Process. 17 (1), 53–69.
Mairal, J., Sapiro, G., Elad, M., 2008b. Learning multiscale sparse representations for image and video restoration. SIAM Multiscale Model. Simul. 7 (1), 214–241.
Maji, S., Berg, A.C., Malik, J., 2008. Classification using intersection kernel support vector machines is efficient, in: IEEE Conf. Comp. Vis. Pattern Recog., pp. 1–8.
Malvehy, J., Puig, S., Argenziano, G., Marghoob, A.A., Soyer, H.P., 2007. Dermoscopy report: proposal for standardization: results of a consensus meeting of the international dermoscopy society. J. Am. Acad. Dermatol. 57 (1), 84–95.
Marchetti, M.A., Codella, N.C.F., Dusza, S.W., Gutman, D.A., Helba, B., Kalloo, A., Mishra, N., Carrera, C., Celebi, M.E., DeFazio, J.L., Jaimes, N., Marghoob, A.A., Quigley, E., Scope, A., Yelamos, O., Halpern, A.C., 2018. Results of the 2016 international skin imaging collaboration international symposium on biomedical imaging challenge: Comparison of the accuracy of computer algorithms to dermatologists for the diagnosis of melanoma from dermoscopic images. J. Am. Acad. Dermatol. 78 (2), 270–277.
Marghoob, A.A., Koenig, K., Bittencourt, F.V., Kopf, A.W., Bart, R.S., 2000. Breslow thickness and Clark level in melanoma. Cancer 88 (3), 589–595.
Marin, C., Alferez, G., Cordova, J., Gonzalez, V., Detection of melanoma through image recognition and artificial neural networks, in: World Cong. Med. Physics Biomed. Eng., pp. 832–835.
Matsunaga, K., Hamada, A., Minagawa, A., Koga, H., 0000. Image classification of melanoma, nevus and seborrheic keratosis by deep neural network ensemble, CoRR arxiv.org/abs/1703.03108.
Mayoclinic, 2017a. How skin cancer develops. http://www.mayoclinic.org/diseases-conditions/skin-cancer/multimedia/melanoma/vid-20084739. (Accessed 13 September 2017).
Mayoclinic, 2017b. Mayo clinic - melanoma. http://www.mayoclinic.org/diseases-conditions/melanoma/basics/definition/con-20026009. (Accessed 4 July 2017).
Medicine Net, 2017. What is melanoma? http://www.medicinenet.com/melanoma/article.htmwhat-is-melanoma. (Accessed 4 July 2017).
Meier, L., Geer, S.V.D., Buhlmann, P., 2008. The group lasso for logistic regression. J. R. Stat. Soc. Ser. B Stat. Methodol. 70 (1), 53–71.
Melanoma.Org, 2017. Melanoma facts and statistics. https://www.melanoma.org.au/understanding-melanoma/melanoma-facts-and-statistics/.(Accessed 4 July 2017).
Melgani, F., 2006. Robust image binarization with ensembles of thresholding algorithms. Elec. Imag. 15 (2), 15–15–11.
Melli, R., Grana, C., Cucchiara, R., 2006. Comparison of color clustering algorithms for segmentation of dermatological images. In: SPIE Med. Imag.. pp. 61443S–61443S.
Mendonca, T., Ferreira, P.M., Marques, J.S., Marcal, A.R., Rozeira, J., 2015. PH2 –A public database for the analysis of dermoscopic images. In: Dermoscopy Image Anal.. pp. 419–439
Menegola, A., Fornaciali, M., Pires, R., Bittencourt, F.V., Avila, S., Valle, E., 2017a. Knowledge transfer for melanoma screening with deep learning, in: IEEE Int. Symp. Biomed. Imag., pp. 297–300.
Menegola, A., Tavares, J., Fornaciali, M., Li, L.T., Avila, S., Valle, E., 2017bRECOD Titans at ISIC Challenge, CoRR arxiv.org/abs/1703.04819.
Mete, M., Kockara, S., Aydin, K., 2011. Fast density-based lesion detection in dermoscopy images. Comput. Med. Image Graph. 35 (2), 128–136.
Mishra, N., Celebi, M.E., 2016. An overview of melanoma detection in dermoscopy images using image processing and machine learning.
Naing, A., Hajjar, J., 2017. Immunotherapy. Springer.

Ng, V.T., Fung, B.Y., Lee, T.K., 2005. Determining the asymmetry of skin lesion with fuzzy borders. Comput. Biol. Med. 35 (2), 103–120.
Nobuyuki, O., 1979. A threshold selection method from gray-level histograms. IEEE Trans. Syst. Man. Cybern. Syst. 9 (1), 62–66.
Noh, H., Hong, S., Han, B., 2015. Learning deconvolution network for semantic segmentation, in: IEEE Int. Conf. Computer Vis., 2015, pp. 1520–1528.
Ogorzalek, M., Nowak, L., Surowka, G., Alekseenk, A., 2011. Modern techniques for computer-aided melanoma diagnosis. In: Melanoma in the Clinic - Diagnosis, Management and Complications of Malignancy. INTECH.
Oktar, Y., Turkan, M., 2018. A review of sparsity-based clustering methods. ELSEVIER Signal Process. 148 (2018), 20–30.
Parikh, R., Mathai, A., Parikh, S., Chandra, S.G., Thomas, R., 2008. Understanding and using sensitivity, specificity and predictive values. Indian J. Ophthalmol. 56 (1), 45–50.
Patel, S., Eluri, M., Boyers, L.N., Karimkhani, C., Dellavalle, R.P., 2014. Update on mobile applications in dermatology. Dermatol. Online J. 21 (2).
Pathak, D., Krahenbuhl, P., Darrell, T., 2015. Constrained convolutional neural networks for weakly supervised segmentation, in: IEEE Int. Conf. Computer Vis., pp. 1796–1804.
PDQ Adult Treatment Editorial Board, (2018a). PDQ Melanoma treatment. https://www.cancer.gov/types/skin/patient/melanoma-treatment-pdq. (Accessed 13 February 2018). [PMID: 26389388].
PDQ Adult Treatment Editorial Board, (2018b). https://www.cancer.gov/publications/pdq/editorial-boards/adult-treatment. (Accessed 3 December 2018).
Peotta, L., Granai, L., Vandergheynst, P., 2006. Image compression using an edge adapted redundant dictionary and wavelets. Signal Process. 86 (3), 444–456.
Peyre, G., 2009. Sparse modeling of textures. J. Math. Image Vis. 34 (1), 17–31.
Priddy, K.L., Keller, P.E., 2005. Artificial Neural Networks: An Introduction. SPIE.
Protter, M., Elad, M., 2009. Image sequence denoising via sparse and redundant representations. IEEE Trans. Image Process. 18 (1), 27–35.
Quintana, J., Garcia, R., Neumann, L., 2009. A novel method for color correction in epiluminescence microscopy. Comput. Med. Image Graph. 35 (7), 646–652.
Real, R., Vargas, J.M., 1996. The probabilistic basis of Jaccard's index of similarity. Syst. Biol. 45 (3), 380–385.
Robertson, S., 2008. A new interpretation of average precision, in: Int. ACM SIGIR Conf. Res. Dev. Info. Ret., pp. 689–690.
Ronneberger, O., Fischer, P., Brox, T., 0000. U-net: Convolutional networks for biomedical image segmentation, CoRR arxiv.org/abs/1505.04597.
Rubegni, P., Cevenini, G., Burroni, M., Perotti, R., Dell'Eva, G., Sbano, P., Miracco, C., 2002. Automated diagnosis of pigment skin lesions. Int. J. Cancer 101 (6), 576–580.
Russakovsky, O., Deng, J., Su, H., Krause, J., Satheesh, S., Ma, S., Huang, Z., Karpathy, A., Khosla, A., Bernstein, M., Berg, A.C., Fei-Fei, L., 2015. Imagenet large scale visual recognition challenge. Int. J. Comput. Vision 115 (3), 211–252.
Santy, A., Joseph, R., 2015. Segmentation methods for computer aided melanoma detection, in: Global Conf. Communication Tech., pp. 490–493.
Schmid, P., 1999. Segmentation of digitized dermatoscopic images by two-dimensional color clustering. IEEE Trans. Med. Imaging 18 (2), 164–171.
Schmid, C., 2001. Constructing models for content-based image retrieval, in: IEEE Comp. Soc. Conf. Comp. Vis. Pattern Recog. Vol. 2, pp. 39–45.
Sci-Kit Learn, 2017. SVM with RBF kernel. http://scikit-learn.org/stable/auto_examples/svm/plot_rbf_parameters.html. (Accessed 19 July 2017).
Senel, E., 2011. Dermatoscopy of non-melanocytic skin tumors. Indian J. Dermatol. Venereol. Leprol. 77 (1), 16–22.
Sermanet, P., Eigen, D., Zhang, X., Mathieu, M., Fergus, R., Cun, Y. L-., 0000. Overfeat: Integrated recognition, localization and detection using convolutional networks, CoRR arxiv.org/abs/1312.6229.
Setio, A.A.A., Ciompi, F., Litjens, G., Gerke, P., Jacobs, C., van Riel, S.J., Wille, M.M.W., Naqibullah, M., Sanchez, C.I., Ginneken, B.V., 2016. Pulmonary nodule detection in ct images: false positive reduction using multi-view convolutional networks. IEEE Trans. Med. Imaging 35 (5), 1160–1169.
Sezgin, M., Sankur, B., 2004. Survey over image thresholding techniques and quantitative performance evaluation. J. Electron. Imaging 13 (1), 146–165.
Shapiro, L.G., Stockman, G.C., 2002. Computer Vision. Prentice Hall.
Shelhamer, E., Long, J., Darrell, T., 0000. Fully convolutional networks for semantic segmentation, CoRR arxiv.org/abs/1605.06211.
Shin, H.-C., Roth, H.R., Gao, M., Lu, L., Xu, Z., Nogues, I., Yao, J., Mollura, D., Summers, R.M., 2016. Deep convolutional neural networks for computer-aided detection: cnn architectures, dataset characteristics and transfer learning. IEEE Trans. Med. Imaging 35 (5), 1285–1298.
Siegel, R.L., Miller, K.D., Jemal, A., 2018. Cancer statistics. CA: A Cancer J. Clinicians 68 (1), 7–30.
Simonyan, K., Zisserman, A., 2015. Very deep convolutional networks for large-scale image recognition. In: ICLR.
Situ, N., Yuan, X., Chen, J., Zouridakis, G., Malignant melanoma detection by bag-of-features classification, in: IEEE Int. Conf. Eng. Med. Biol. Soc., pp. 3110–3113.
SkinCancer.Org, 2017. Skin cancer facts and statistics. http://www.skincancer.org/skin-cancer-information/skin-cancer-facts. (Accessed 4 July 2017).
SLATMD, 2017f. https://challenge.kitware.com/#challenge/n/ISIC_2017%3A_Skin_Lesion_Analysis_Towards_Melanoma_Detection. (Accessed 19 July 2017).
Smith, L.N., Topin, N., 0000. Deep convolutional neural network design patterns, CoRR arxiv.org/abs/1611.00847.
SPAMS, 2017g. http://spams-devel.gforge.inria.fr/. (Accessed 8 October 2017).
Steinwart, I., Christmann, A., 2008. Support Vector Machines. Springer.
Szegedy, C., Ioffe, S., Vanhoucke, V., 0000. Inception-v4 inception-resnet and the impact of residual connections on learning, CoRR arxiv.org/abs/1602.07261.
Tajbakhsh, N., Shin, J.Y., Gurudu, S.R., Hurst, R.T., Kendall, C.B., Gotway, M.B., Liang, J., 2016. Convolutional neural networks for medical image analysis: Full training or fine tuning? IEEE Trans. Med. Imaging 35 (5), 1299–1312.
Tang, Y., 2013. Deep learning using linear support vector machines. In: ICML.
Tenenhaus, A., Nkengne, A., Horn, J., Serruys, C., Giron, A., Fertil, B., 2010. Detection of melanoma from dermoscopic images of naevi acquired under uncontrolled conditions. Skin Res. Technol. 16 (1), 85–97.
Tkalcic, M., Tasic, J.F., 2003. Colour spaces: perceptual, historical and applicational background. In: IEEE EUROCON Computer As a Tool, Vol. 1. pp. 304–308.
Vang, J.W., Chapman, L.W., Keller, M.S., 2017. Challenges to smartphone applications for melanoma detection. Dermatol. Online J. 23 (2).
Washington, C.M., Leaver, D.T., 2016. Principles and Practice of Radiation Therapy. Elsevier.
WebMd, 2017. ABCDEs of melanoma skin cancer. http://www.webmd.com/melanoma-skin-cancer/abcds-of-melanoma-skin-cancer. (Accessed 4 July 2017).
WHO, 2017. Skin cancers. http://www.who.int/uv/faq/skincancer/en/index1.html. (Accessed 13 September 2017).
Wight, P., Lee, T.K., Lui, H., Atkins, M.S., 2011. Chromatic aberration correction: an enhancement to the calibration of low-cost digital dermoscopes. Skin Res. Technol. 17 (3), 339–347.
Wolf, J.A., Moreau, J.F., Akilov, O., Patton, T., English, J.C., Ho, J., Ferris, L.K., 2013. Diagnostic inaccuracy of smartphone applications for melanoma detection. JAMA Dermatol. 149 (4), 422–426.
Wong, A., 2011. Automatic skin lesion segmentation via iterative stochastic region merging. IEEE Trans. Info. Tech. Biomed. 15 (6), 929–936.
Wu, Y., Xie, F., Jiang, Z., Meng, R., 2013. Automatic skin lesion segmentation based on supervised learning, in: Int. Conf. Imag. Graph., pp. 164–169.
Yan, L., Rosen, N., Arteaga, C., 2011. Targeted cancer therapies. Chin. J. Cancer 30 (1), 1–4.
Yu, L., Chen, H., Dou, Q., Qin, J., Heng, P.A., 2017. Automated melanoma recognition in dermoscopy images via very deep residual networks. IEEE Trans. Med. Imaging 36 (4), 994–1004.
Yuan, Y., Chao, M., Lo, Y.-C., 0000. Automatic skin lesion segmentation with fully convolutional-deconvolutional networks, CoRR arxiv.org/abs/1703.05165.
Yuan, X., Situ, N., Zouridakis, G., 2009. A narrow band graph partitioning method for skin lesion segmentation. Pattern Recognit. 42 (6), 1017–1028.
Yuksel, M.E., Borlu, M., 2009. Accurate segmentation of dermoscopic images by image thresholding based on type-2 fuzzy logic. IEEE Trans. Fuzzy Syst. 17 (4), 976–982.
Zhou, Y., Song, Z., 2013. Binary decision trees for melanoma diagnosis, in: Int. W. Multiple Classifier Syst., pp. 374–385.
Zhou, Y., Song, Z., 2014. Melanoma diagnosis with multiple decision trees, in: Comp. Vis. Tech. Diag. Skin Cancer, pp. 267–282.